Phenotypic adaptation of Pseudomonas aeruginosa in the presence of siderophoreantibiotic conjugates during epithelial cell infection

Quentin Perraud, Paola Cantero, Mathilde Munier, Françoise Hoegy, Nicolas Zill, Véronique Gasser, Gaëtan L A Mislin, Laurence Ehret-Sabatier, Isabelle J Schalk

Phenotypic adaptation of *Pseudomonas aeruginosa* in the presence of siderophore-antibiotic conjugates during epithelial cell infection

Quentin PERRAUD[1,2], Paola CANTERO[3], Mathilde MUNIER[1,2], Françoise HOEGY[a,b], Nicolas ZILL[1,2], Véronique GASSER[1,2], Gaëtan L. A. MISLIN[1,2], Laurence EHRET-SABATIER[3], and Isabelle J. SCHALK[1,2*]

[1] Université de Strasbourg, InnoVec, UMR7242, ESBS, Bld Sébastien Brant,
F-67413 Illkirch, Strasbourg, France

[2] CNRS, UMR7242, ESBS, Bld Sébastien Brant,
F-67413 Illkirch, Strasbourg, France

[3] Laboratoire de Spectrométrie de Masse BioOrganique, Université de Strasbourg, CNRS, IPHC UMR 7178, F-67000 Strasbourg, France

[*] To whom correspondence should be addressed: schalk@unistra.fr.

Running title: *P. aeruginosa* adaptation to siderophore-antibiotics

Abstract

Iron is an essential nutrient for bacterial growth. Thus, iron acquisition pathways have often been considered to be gateways for the uptake of antibiotics into bacteria. Bacteria excrete chelators, called siderophores, to access iron. Antibiotic molecules can be covalently attached to siderophores for their transport into pathogens during the iron-uptake process. *P. aeruginosa* carries genes for at least 20 different iron-uptake strategies, using various siderophores, within its genome. Although it produces the two siderophores pyoverdine and pyochelin, it is also able to use many siderophores produced by other bacteria. We investigated the phenotypic plasticity of iron-uptake pathway expression in an epithelial cell infection assay in the presence of two different siderophore-antibiotic conjugates, one with a hydroxamate siderophore and the second with a tris-catechol. Proteomic and RT-qPCR approaches showed that *P. aeruginosa* was able to sense the presence of both compounds in its environment and adapt the expression of its iron uptake pathways to access iron via them. In parallel, expression of the proteins of the pyochelin pathway was significantly repressed, as well as that of proteins of the pyoverdine pathway, but to a lesser extent. Interestingly, the transcription and expression of several virulence factors was also repressed in the presence of both siderophore-antibiotic conjugates. The catechol-type siderophore-antibiotic conjugates were clearly more efficient in inducing the expression of their corresponding transporter than the hydroxamate compound when both were simultaneously present in the environment of the pathogen, indicating that catechol-type siderophores are more promising vectors for antibiotic vectorization using a Trojan-horse strategy.

Introduction

Antibiotic resistance is a complex and growing problem for human health. In 2017, the World Health Organization published a list of highly resistant bacteria for which new antibiotics are urgently needed. The most critical pathogens on this list are Gram-negative bacteria, such as *Acinetobacter*, *Pseudomonas*, and various enterobacteria (including *Klebsiella*, *E. coli*, *Serratia*, and *Proteus*). The bottleneck in the development of new antibiotics for Gram-negative bacteria is the need for these drugs to cross the outer membrane. The use of nutrient-importation pathways as gateways for the uptake of antibiotics has often been proposed to bypass the low permeability of the Gram-negative cell wall (1).

Iron is a key nutrient, as this metal is involved in many crucial biological processes, and is therefore essential for bacterial growth and virulence. To access iron, bacteria produce siderophores, small molecules with a very high affinity for ferric iron (2). These iron chelators are synthesized by bacteria and released into their environment to scavenge iron. The ferric complexes that are formed are recovered by specific transporters (3). Antibiotics can be covalently linked to siderophores with the idea they will be transported into the pathogens during the ferri-siderophore uptake process – referred to as a Trojan-horse strategy (1, 4, 5). One such siderophore-antibiotic conjugate (Cefiderocol), developed by Shionogi, was approved by the US Food and Drug Administration in November 2019 for the treatment of complicated urinary tract infections, showing that Trojan-horse strategies can be successful (6). Moreover, evolution has also developed natural siderophore-antibiotic conjugates (also called sideromycins), demonstrating the relevance of such a strategy. The archetypes among sideromycins are albomycins (7, 8), ferrimycins (9), danomycins (10), and salmycins (11), isolated mainly from streptomycetes or actinomycetes and produced to kill other microorganisms and dominate a given microbiota.

One major bottleneck limiting the development of siderophore-antibiotic conjugates is that all bacteria are equipped with several iron-uptake pathways. Consequently, bacteria can switch off the expression of the targeted iron uptake pathway and express an alternative one, possibility leading to the rapid development of resistance strategies. For example, *P. aeruginosa* carries genes within its genome for at least 20 different iron-uptake strategies (12): (i) one ferrous (Fe^{2+}) iron uptake pathway, (ii) three heme acquisition pathways, (iii) ferric iron (Fe^{3+}) uptake pathways by the two siderophores pyoverdine (PVD) and pyochelin (PCH), produced by the pathogen itself, and (iv) at least 10 different "siderophore piracy" strategies to uptake Fe^{3+} using exosiderophores (siderophores produced by other bacteria). Indeed, most bacteria can use siderophores produced by other bacteria in multispecies communities and during infections by expressing compatible transporters that are able to capture and import ferric complexes they cannot synthesize themselves (13–16). Except for ferrous-iron uptake, bacterial iron-uptake pathways always include an outer membrane transporter (OMT) involved in ferri-siderophore or heme uptake, enzymes involved in iron release from the siderophore or heme, and inner membrane transporters (ABC transporters of protonmotive force-dependent permeases). These proteins, especially the OMTs, are always specific for one siderophore or a family of structurally-related siderophores (3, 17). Consequently, bacteria able to access iron via several siderophores carry genes within their genome that encode an OMT specific for each siderophore (3).

In contrast to the large amount of genomic data generated by bacterial genome sequencing, almost no data are available concerning the phenotypic plasticity associated with the expression of these various iron-uptake pathways. Uptake pathways are considered to be generally expressed at a basal level and pathogens only induce the expression of the most efficient pathway(s) for iron acquisition depending on the bacterial environment (16). It has

also been shown that bacteria are often able to sense the presence of exosiderophores and express the corresponding transporters, allowing them to access iron via these exosiderophores (16, 18–22). Bacteria are also able to switch from the expression of one iron-uptake pathway to another in response to synthetic iron chelators, as shown for *P. aeruginosa* cells with an analogue of the siderophore enterobactin (ENT) (23). Recently, we showed by proteomics and RT-qPCR that tris-catechol type siderophores, such as ENT or vibriobactin (VIB), induce the transcription and expression of the genes involved in their corresponding uptake pathways in *P. aeruginosa* more efficiently than tris-hydroxamate siderophores, such as ferrichrome (16). The data also showed that the presence of different iron uptake pathways in the genome of a pathogen involves high phenotypic plasticity in response to diverse environmental stimuli (16). Such phenotypic plasticity plays a key role in the ability of siderophore-antibiotic conjugates to be transported efficiently into the target bacteria. If the right uptake pathway is not expressed, the drugs have no chance of being efficiently transported into the bacteria by their associated siderophore.

Here, we investigated, for the first time, the phenotypic adaptation of *P. aeruginosa* to the presence of two different siderophore-antibiotic conjugates in an epithelial cell infection assay using proteomics and RT-qPCR. We used the natural sideromycin albomycin (ALBO) (Fig 1A), for which the siderophore component is similar to ferrichrome (FERRI), a siderophore that chelates iron via three hydroxamate groups. For the second conjugate, we used the synthetic compound TCVL6, corresponding to linezolid vectorized by a tris-catechol siderophore (TCV) analogue of ENT (Fig 1A). Both compounds have no antibiotic activity on the pathogen at the concentrations used here (25, 26) and could therefore be used as tools to investigate how the bacteria adapts the expression of its various iron-uptake pathways in the presence of such Trojan-horse compounds. We show that both compounds are able to

promote *P. aeruginosa* growth in iron-restricted conditions, ALBO by the FERRI-dependent uptake pathway (Fig 1B) and TCVL6 by the ENT-dependent uptake pathway (Fig 1C). Both compounds were able to induce the transcription and expression of the genes encoding proteins involved in their corresponding uptake pathways, indicating that *P. aeruginosa* PAO1 is able to sense the presence of these two compounds and use them to access iron. This occurred in parallel with a decrease in the transcription and expression of the proteins of the endogenous siderophore-dependent iron uptake pathways (PVD and PCH), as well as that of virulence factors. Finally, when bacteria were simultaneously in the presence of both ALBO and TCVL6, the proteins of the ferri-TCVL6 uptake pathway were more highly expressed than those of the ferri-ALBO uptake pathway, indicating that between the two compounds, *P. aeruginosa* preferentially uses TCVL6 to access iron.

Results

Ability of ALBO and TCVL6 to compete for iron with PVD. The efficient uptake of siderophore-antibiotic conjugates into bacteria requires that various conditions be met. Among them, the siderophore moiety must have a high affinity for iron and be able to compete for this metal with other siderophores that may be present in the bacterial environment, such as the siderophores produced by the pathogens themselves. *P. aeruginosa* produces two siderophores, PVD and PCH, with PVD having a higher affinity for iron than PCH (K_a of $10^{30.8}$ M^{-1} for PVD vs 10^{18} M^{-2} for PCH (27, 28)). Apo PVD also has specific spectral properties, with a characteristic absorbance peak at 400 nm (pH 7.0) and fluorescence emission at 447 nM, whereas its fluorescence is quenched when complexed with iron (27, 29). As we have described previously, these spectral properties can be used to compare the ability of various chelators to scavenge iron (16). Here we used them to monitor the competition between PVD and the compounds FERRI, ALBO, TCV, and TCVL6 for iron (Fig 2). PVD-Fe (non-fluorescent) at 10 µM was incubated in the presence of increasing concentrations of apo FERRI, ALBO, TCV, and TCVL6 (Fig 2A). The complete removal of iron from PVD was only observed for the catechol-type compounds (TCV and TCVL6) at concentrations of approximately 20 µM (two-fold excess compared to PVD-Fe; Fig 2A). Neither FERRI nor ALBO were able to completely remove iron from PVD at the concentrations tested, (70 – 80% of the PVD was still in its ferric form, Fig 2A), indicating that these compounds compete less efficiently for the scavenging of iron than catechol-type siderophores or conjugates. We also monitored the kinetics of PVD-Fe dissociation by incubating 10 µM PVD-Fe with 100 µM FERRI, ALBO, TCV, or TCVL6 (Fig 2B) and confirmed that catechol-type compounds clearly compete more efficiently for iron with PVD than hydroxamate molecules. These data are consistent with the affinities of these families of siderophores for iron: K_a of 10^{49} M^{-1} for ENT(30), an analogue of TCV, 10^{29} M^{-1} for

FERRI (31), and $10^{30.8}$ M^{-1} for PVD (27). Furthermore, they show that the presence of the antibiotic moiety does not significantly affect the chelation properties of the vector moiety.

ALBO and TCVL6 both transport iron into P. aeruginosa cells. Previous studies have shown that ENT and FERRI are both able to transport Fe into bacteria via the OMT PfeA for ENT and FiuA for FERRI (14, 23, 32). Moreover, previous proteomic and RT-qPCR analyses of *P. aeruginosa* grown in iron-restricted medium have shown that TCV is also able to enter *P. aeruginosa* cells via the OMT PfeA, as the presence of this compound induces the expression of PfeA and PfeE, two proteins of the ENT-Fe uptake pathway (23). Such induction involves an interaction with the inner membrane sensor PfeS of the two-component system PfeS/PfeR (18, 23). We used the same approach here. *P. aeruginosa* PAO1 cells were grown in the presence of TVCL6 and the transcription of *pfeA* and *pfeE* analyzed by RT-qPCR (Fig 3A). We observed induction of the transcription of the *pfeA* and *pfeE* genes in the presence of TCVL6 with an efficiency equivalent to that for the vector TCV, without the antibiotic component, and higher efficiency than that for ENT. Such induction of *pfeA* and *pfeE* transcription is a proof that TCVL6 is able to cross the outer membrane of *P. aeruginosa* cells and interact with the two-component system PfeS/PfeR in the periplasm.

Nothing has been described in the literature about the ability of ALBO to transport iron into *P. aeruginosa* cells. Consequently, we carried out an ^{55}Fe uptake assay on iron-starved *P. aeruginosa* cells that were unable to produce PVD or PCH (Δ*pvdF*Δ*pchA* strain (23)) with ALBO as a siderophore (Fig 3B). The Δ*pvdF*Δ*pchA* mutant was used to avoid any iron uptake via the siderophores produced by the bacteria itself. We observed an uptake rate of 150 pmol ^{55}Fe transported per $OD_{600\ nm}$ per min, showing that ALBO is able to transport iron into *P. aeruginosa* cells. Uptake was completely abolished in the presence of CCCP, a protonmotive

force inhibitor (33), indicating that such uptake is not due to diffusion via porins across the outer membrane but is TonB-dependent. TonB is an inner-membrane protein that spans into the periplasm and provides the energy to the ferri-siderophore OMTs for uptake across the outer membrane (34, 35). The deletion of *fiuA* (FERRI OMT) resulted in 40% inhibition of ^{55}Fe uptake at 1 h and 15% at 3 h. FoxA has also been described as a OMT for hydroxamate siderophores (14, 32) but its deletion had no effect on ^{55}Fe accumulation via ALBO. These data show that ferric iron-loaded ALBO uptake occurs via FiuA and at least one other OMT.

We evaluated the ability of ALBO and TCVL6 to provide bacteria with iron by also carrying out growth assays on *P. aeruginosa* cells unable to produce PVD or PCH (Δ*pvdF*Δ*pchA* strain) in iron-restricted CAA medium, in the presence or absence of 10 µM ENT, TCV, TCVL6, FERRI, or ALBO. The same assays were also carried out with various OMT mutants to identify the transporter involved in such uptake. As these growth assays were carried out using strains unable to produce siderophores, all iron present in the media was scavenged by ENT, TCV, TCVL6, FERRI, or ALBO. Consequently, bacteria only grew if they expressed the OMT necessary to import the ferric forms of these compounds. The Δ*pvdF*Δ*pchA* strain grew in the presence of all tested compounds (Fig 4), showing that *P. aeruginosa* is able to access iron by using them as siderophores and that neither ALBO nor TCVL6 had antibiotic activity at the concentrations tested. Growth was still observed in the presence of ENT, TCV, and TCVL6 with the Δ*pvdF*Δ*pchA*Δ*pfeA* and Δ*pvdF*Δ*pchA*Δ*pirA* mutants, but not Δ*pvdF*Δ*pchA*Δ*pfeA*Δ*pirA* cells, indicating that both PfeA and PirA are involved in iron uptake by these three compounds. Both transporters had to be deleted to stop the bacteria from growing in the presence of the catechol compounds. Concerning FERRI and ALBO, we observed growth for the four strains tested Δ*pvdF*Δ*pchA*, Δ*pvdF*Δ*pchA*Δ*fiuA*, Δ*pvdF*Δ*pchA*Δ*foxA* and Δ*pvdF*Δ*pchA*Δ*foxA*Δ*fiuA* (FoxA being involved in the uptake of the ferri-nocardamine complex, a tris-hydroxamate

siderophore (32)), showing that although FiuA is able to transport iron into bacteria (Fig 3B), at least one other unidentified OMT can perform the same function and it is not FoxA.

In conclusion, ENT, TCV, and TCVL6 are able to transport iron into *P. aeruginosa* cells via the OMTs PfeA and PirA and FERRI and ALBO by FiuA and another unidentified OMT.

***The presence of siderophore-antibiotic conjugates induces the transcription and expression of their corresponding OMTs in P. aeruginosa cells infecting epithelial cells*.** It is well documented that bacteria are able to sense the presence of exosiderophores in their environment, consequently leading to induction of the transcription and expression of their corresponding OMTs (16, 18–22). We have previously shown that the presence of either TCV or ENT in planktonic cultures of *P. aeruginosa* induces the transcription and expression of the OMT *pfeA* and the presence of FERRI, the OMT *fiuA* (16, 23). Proteomic and RT-qPCR approaches have shown that *P. aeruginosa* is also able to sense the presence of exosiderophores and subsequently adapt its phenotype in even more complex systems, such as an epithelial infection assay (16). We used the same approach here to investigate whether *P. aeruginosa* PAO1 senses the presence of ALBO and TCVL6 in an epithelial cell infection assay.

We first used a proteomic approach to identify the bacterial proteins, especially the OMTs, showing differential expression in the presence of ALBO or TCVL6 (Fig 5) and then RT-qPCR to confirm the proteomic results and compare the levels of transcription of the different genes (Fig 6). Epithelial A549 cells were infected with *P. aeruginosa* PAO1 cells grown overnight in LB (conditions under which the iron-uptake pathways are poorly expressed (16)). The bacteria/epithelial cell ratio used resulted in 40 to 50% viability of the cells 10 h after infection, as we previously described in Perraud *et al.*, 2020 (16). Only bacteria associated with

226 the epithelial cells were harvested for proteomic analysis, after 3 h of infection, when we
227 started to observe apoptosis of the epithelial cells. The sample preparation and proteomic
228 workflow used allowed the identification of 1,300 proteins from *P. aeruginosa* in the presence
229 of a large number of proteins from the epithelial cells.

230 Proteomic and RT-qPCR data (Figs 5 and 6) showed the presence of either TCVL6, TCV,
231 or ENT to strongly induce the expression of PfeA (log_2 fold change of 4.61 for proteomics and
232 4.71 for RT-qPCR for TCVL6). The expression of PfeE (gene number PA2689, esterase
233 hydrolyzing ENT -Fig 1C) was also induced, with a log_2 fold change of 2.60, 2.58 and 0.91 in the
234 proteomic data in the presence of TCVL6, TCV, and ENT. There was also an effect on PirA
235 transcription or expression, by ENT, TCV, and TCVL6 (Figs 3 and 4) with a log_2 fold change of
236 1.83 for TCVL6, 1.70 for TCV and 0.70 for ENT. All three molecules (ENT, TCV, and TCVL6) had
237 a similar effect on the *P. aeruginosa* phenotype, proving that TCVL6 is able to enter the
238 bacterial periplasm, like ENT and TCV, and bind to PfeS, the sensor of the two-component
239 system involved in the regulation of the expression of the ENT-dependent iron-uptake
240 pathway in *P. aeruginosa* cells (18, 23), and showing that the linezolide component linked to
241 TCV does not affect this detection mechanism.

242 The presence of ALBO or FERRI induced the expression of FiuA (log_2 fold change of 5.68
243 for proteomics and 3.03 for RT-qPCR for ALBO) and no other OMT, suggesting that the other
244 unidentified OMT that is involved in iron acquisition by ALBO (Figs 3 and 4) must be either
245 expressed constitutively at sufficiently high levels to allow uptake, regardless of the growth
246 conditions, or its expression is induced only if FiuA cannot be expressed. In addition, in the
247 case of ALBO, the antibiotic component linked to FERRI did not interfere with the molecular
248 mechanisms involving the sigma/anti-sigma system FiuI/FiuR (21) and required for the
249 detection of these ferri-hydroxamate compounds by *P. aeruginosa*.

The data also show that all five compounds strongly repress the expression of the various proteins of the PCH pathway, such as the OMT FptA (mean log_2 fold change of -3.16 for the proteomic data) as well as the enzymes involved in PCH biosynthesis (mean log_2 fold change of -2.92 for all enzymes) (Fig 5B). The expression of the proteins of the PVD pathway was more strongly repressed by ALBO than the other compounds tested, with FERRI and TCVL6 having almost no effect on the transcription and expression of these genes (Fig 5B). As most of the proteins in the Fur regulon appeared to also be under-expressed in the presence of ALBO relative to the other compounds tested (S1 Fig), this phenotype is certainly due to low-level iron contamination of ALBO that probably had an impact on the Fur regulon as a whole.

In conclusion, *P. aeruginosa* is able to detect the two siderophore-conjugates used in this study (ALBO and TCVL6) in its growth environment, even in a complex system such as an epithelial infection assay, and clear phenotypic adaption is observed. Both compounds were able to induce the transcription and expression of their corresponding OMT in *P. aeruginosa* cells: FiuA for ALBO and PfeA for TCVL6. The phenotypic adaptation of *P. aeruginosa* in this infection assay also involved repression of the transcription and expression of the proteins of the PCH and PVD pathways.

Siderophore-antibiotic conjugates also affect the expression of virulence factors. Transcription of the genes of the PVD pathway is regulated by two sigma factors, FpvI and PvdS, the second also regulating the transcription of virulence factors such as exotoxin A (ToxA) (36, 37), a major virulence factor of *P. aeruginosa* and Piv (also called PrpL) endoprotease (38, 39). The alkaline protease AprA is regulated by OxyR and is thus dependent on redox stress, which can be induced by high iron concentrations (40). Thus, we

also performed proteomic analysis of the expression of all virulence factors expressed by *P. aeruginosa* cells during the infection of A549 cells (Fig 7A). However, all secreted virulence factors could not be detected with the protocol used to harvest the *P. aeruginosa* cells after infection. Consequently, we used RT-qPCR to evaluate the infected samples for the transcription of the genes encoding virulence factors for which their transcription is regulated or not by PvdS or OxyR (Fig 7B), as well as several other virulence factors, such as AmrZ, a transcriptional regulator that controls the expression of many genes involved in environmental adaptation (41), PhzA2, a flavin-containing monooxygenase involved in phenazine biosynthesis (42, 43), and, finally, secreted virulence factors such as ExoY, a protease injected into eukaryotic cells by the type III secretion system (44–47) and the LasB elastase (48).

Proteomic analyses showed repression of the expression of many virulence factors, mostly in the presence of ALBO, but also FERRI, ENT, and TCV, and, to a lower extent, TCVL6 (Fig 7). The lower effect of TCVL6 can be explained by the slightly lower solubility of this compound. Indeed, in some cases, a small amount of precipitate of TCVL6 could be observed. In addition, RT-qPCR showed different transcriptional profiles of the tested virulence factors in the presence of ENT, TCVL6, and ALBO. The presence of ENT mostly repressed the transcription of *aprA* and *toxA*, as the expression of these virulence factors is regulated by PvdS. TCVL6 also repressed the transcription of *aprA* (more strongly than ENT) and *toxA*, as well as the transcription of *piv* and *phzA2*. Finally, ALBO repressed the transcription of *aprA*, *exoY*, *piv*, and *toxA*.

A tris-catechol conjugate more efficiently induces the transcription of its OMT than a hydroxamate conjugate in P. aeruginosa cells infecting epithelial cells. We have previously

298 shown that *P. aeruginosa* cells infecting epithelial A549 cells increase the transcription and
299 expression of catechol siderophore-dependent iron-uptake pathways, and not those of
300 hydroxamate siderophores, in the presence of a mixture of four different siderophores (16).
301 Here, the infection assay was repeated with a mixture of either TCV and FERRI or TCVL6 and
302 ALBO and analyzed by RT-qPCR (Fig 8). The presence of a mixture of FERRI and TCV in the
303 infection assay strongly induced the transcription of *pfeA* (ENT OMT), with a $\log_2$ fold change
304 of 5; *fiuA* (FERRI OMT) transcription being almost not induced (Fig 8A). In addition, we
305 observed repression in the range of a 0.95 – 1.8 $\log_2$ fold change for *fptA*, *fpvA,* and *hasR*
306 expression (the OMTs of PCH, PVD, and the HasA hemophore, respectively). In the presence
307 of a mixture of ALBO and TCVL6, only *pfeA* transcription was strongly induced ($\log_2$ fold change
308 of 5.2), that of *fiuA* almost not at all, and that of *fptA*, *fpvA,* and *hasR* repressed, with a of 0.5
309 – 0.9 $\log_2$ fold change. As the various genes involved in iron acquisition by a given siderophore
310 are always in an operon, a change in the transcription and expression of the gene encoding an
311 OMT implies a similar change for the transcription and expression of the other genes present
312 in the operon.
313 In conclusion, the data show that conjugates with a catechol-type siderophore moiety
314 have more chances to induce their corresponding OMT and consequently their corresponding
315 uptake pathway than hydroxamate vectors.
316
317 ***Long-term effect of TCVL6 compounds on P. aeruginosa cells.*** A recurrent question in the field
318 of siderophore-antibiotic conjugates is how long bacteria can be treated with such compounds
319 before resistance appears. This issue is complex because resistance can appear at different
320 levels. Here, we investigated how long *P. aeruginosa* retains a phenotype that allows the
321 uptake of iron via TCV without switching to the expression of another phenotype. This assay

could not be carried out for TCVL6 and ALBO because of problems of availability of these compounds in larger amounts. TCV is a vector that can chelate iron (Fig 2) and transport it into *P. aeruginosa* cells (23).

We followed the expression of the ENT-dependent uptake pathway in *P. aeruginosa* cells induced by the presence of 10 µM ENT or TCV for 11 days of culture using a strain that expresses a fluorescently tagged PfeE (*mcherrypfeE* (49)). The *mcherrypfeE* strain expresses mCherry tagged PfeE, with the fluorescent tag inserted in the chromosome at the C-terminus of the protein to maintain expression levels close to those of the wildtype strain (49). Each day, *mcherrypfeE* cells were harvested and resuspended in new CAA medium (iron restricted medium) in the presence of either ENT or TCV. Bacterial growth was followed in parallel with the emission of mCherry fluorescence (emission at 610 nm with excitation at 570 nm). Fluorescence due to mCherry increased in the presence of both ENT and TCV, with exactly the same intensity for both compounds during the 11 days of culture (Fig 9), indicating that PfeE, and consequently PfeA, proteins of the ENT-dependent iron uptake pathway, are expressed at same level in the presence of ENT and TCV. During the 11 days, the phenotype of the *P. aeruginosa* cells, in terms of the expression of the ENT-dependent iron uptake pathway, remained the same.

Discussion

Introducing antibiotics into Gram negative bacteria, such as *P. aeruginosa*, via a Trojan-horse strategy using siderophores as vectors is a promising approach. However there are still several bottlenecks in its development. The high antibiotic activity of natural sideromycins clearly shows that the strategy works and the fact that cefiderocol has been approved by the FDA for use in the treatment of urinary infections is a sign that antibiotic vectorization by siderophores should be explored further by pharmaceutical companies. However, developing such compounds requires extensive knowledge of the molecular mechanisms and regulatory network involved in bacterial siderophore-dependent iron acquisition. Most bacteria carry genes encoding several iron uptake pathways in their genome, allowing very high phenotypic plasticity, depending on the presence or not of exosiderophores or sideromycins. Such phenotypic plasticity of *P. aeruginosa* has been investigated in various growth media and in the presence of several exosiderophores (16). The data show that if siderophores produced by other bacteria (exosiderophores) are present, bacteria induce the expression of the uptake pathway corresponding to the exosiderophore(s) (corresponding OMT and enzymes necessary to release the iron from the siderophore) and, in parallel, repress those corresponding to the endogenous siderophores (16).

Here, we show that this also occurs in the presence of the two siderophore-antibiotic conjugates ALBO and TCVL6 in a complex system (an epithelial cell infection assay) with rapid kinetics (3-h infection with the bacteria having been previously grown in iron-rich media). Both compounds have no antibiotic activities on *P. aeruginosa* on the concentrations used. The bacteria sense the presence of both conjugates in their environment and adapt their phenotypes to access iron *via* the sideromycins that are present. This occurs via auto-loop regulating systems: the two-component system PfeS/PfeR for TCVL6 and the sigma and anti-

364 sigma factors FiuI/FiuR for ALBO. Comparison of the transcription induction levels between
365 FERRI and ALBO and between TCV and TCVL6 for their corresponding OMTs shows that the
366 presence of the antibiotic group on each sideromycin had no inhibitory effect on the
367 regulatory mechanism: the presence of the conjugates was sensed by *P. aeruginosa* with the
368 same efficiency as the vector or corresponding siderophore alone.

369 Such induction of FiuA and PfeA expression occurred in parallel with a decrease in the
370 transcription and expression of (i) the proteins involved in PVD and PCH biosynthesis and ferri-
371 PVD and ferri-PCH uptake and (ii) several virulence factors, especially those regulated by PvdS,
372 the sigma factor that regulates the transcription of the genes involved in PVD production.
373 When the bacteria are transferred from LB medium to the infection assay (A459 cells in RIPM
374 medium) in the presence of ALBO and TCVL6, the bacteria prefer to induce the expression of
375 FERRI and ENT uptake pathways and much less those of their own siderophores PVD and PCH.
376 Moreover, the phenotypic effect induced by the presence of the siderophore-conjugates was
377 not only limited to the expression or not of the iron uptake pathways but also that of virulence
378 factors, as their transcription and expression are tightly interconnected. The ability of
379 siderophore-conjugates to repress the transcription and expression of virulence factors is
380 clearly an asset that has to also be considered in such a Trojan-horse strategy using
381 siderophores as vectors.

382 When the infection assay was carried out in the simultaneous presence of both
383 sideromycins, ALBO and TCVL6 (present in equivalent amounts), the catechol-type vector was
384 clearly more efficient in inducing the expression of its corresponding transporters, PfeA, than
385 that for ferrichrome, because of its strong affinity for iron. Catechol-type compounds are
386 clearly more efficient in competing for iron with PVD than hydroxamate molecules (Fig 2),
387 consistent with the affinities of such families of siderophores for iron: K_a of 10^{49} M^{-1} for ENT

(30), 10^{29} M^{-1} for FERRI (31), and $10^{30.8}$ M^{-1} for PVD (27). Because of their higher affinity for iron, tris-catecholate vectors scavenge iron more efficiently in the bacterial environment than hydroxamate compounds (Fig. 2) and consequently have a higher chance to induce the transcription of their corresponding uptake pathways in the bacteria via the auto-loop regulating systems.

In conclusion, the ability of siderophore-conjugates to be detected by the pathogen in its growth environment, even in a complex system, such as an epithelial infection assay, is a great advantage in Trojan-horse strategies, because it ensures the expression of the needed uptake pathway and suggests that such induction should occur as well in the host during an infection. Moreover, the data show that conjugates with a catechol-type siderophore moiety have a greater chance to induce their corresponding OMT, and consequently their corresponding uptake pathway, than hydroxamate vectors and are potentially more efficient Trojan-horse vectors.

Materials and Methods

Chemicals. Enterobactin (ENT) and ferrichrome (FERRI) were purchase from Sigma-Aldrich. Albomycin δ2 (ALBO) was purchased from EMC Microcollection. Pyoverdine (PVD) was purified from *P. aeruginosa* PAO1 culture supernatants as previously described (50). TCV was synthesized according to previously published protocol (51) and TCVL6 was synthesized as described in Supporting information. The protonophore CCCP (carbonyl cyanide *m*-chlorophenylhydrazone) was purchased from Sigma-Aldrich. $^{55}FeCl_3$ was obtained from Perkin Elmer Life and Analytical Sciences (Billerica, MA, USA), at a concentration of 71.1 mM, with a specific activity of 10.18 Ci/g. RPMI was purchased from Thermo-Fisher.

Bacterial strains, plasmids and growth conditions. The *P. aeruginosa* strains used in this study are all listed in 1SM Table in Supporting information. *P. aeruginosa* strains were grown at 30°C in LB broth. When *P. aeruginosa* strains were grown in iron-restricted conditions, CAA medium was used (casamino acid medium, composition: 5 g L^{-1} low-iron CAA (Difco), 1.46 g L^{-1} K_2HPO_4 $3H_2O$, 0.25 g L^{-1} $MgSO_4$ $7H_2O$).

Iron scavenging from PVD-Fe. Compounds were prepared in solution at 10 mM in DMSO (TCV and TCVL6) or water (FERRI, ALBO and PVD). The competition assay with PVD-Fe was carried out as described previously (16). PVD-Fe is prepared in solution at 10 µM in 100 µL of 100 mM HEPES buffer pH 7.4, and incubated at 25 °C in the presence of increasing concentrations of the tested molecules for 48 h. The fluorescence at 447 nm corresponding to formed apo PVD was monitored (excitation at 400 nm) in a TECAN Infinite M200 plate reader. For the kinetic of iron scavenging from PVD-Fe, PVD-Fe at 10 µM in 100 µL of HEPES buffer was incubated at 25 °C in the presence of 100 µM FERRI, ALBO, ENT or TCVL6. The

fluorescence was monitored in function of time during 1 h in a TECAN Infinite M200 plate reader.

Growth assays in iron-restricted conditions. *P. aeruginosa* strains were first grown overnight at 30°C in LB broth and were then washed, resuspended and cultured overnight at 30°C in CAA medium. Afterwards, bacteria were washed, resuspended in CAA medium at 0.02 OD at 600 nm and distributed in the wells of a 96-well plate (Greiner, U-bottomed microplate) in the absence or presence of 10 µM of FERRI, ALBO, ENT, TCV or TCVL6. The plate was incubated at 30 °C, with shaking, in a Tecan microplate reader (Infinite M200, Tecan) and bacterial growth was monitored at $OD_{600\ nm}$. We calculated the mean of three replicates for each measurement.

Iron uptake. ALBO-^{55}Fe complexes were prepared at ^{55}Fe concentrations of 50 µM, with a ALBO:iron (mol:mol) ratio of 20:1. *P. aeruginosa* strains were first grown overnight at 30°C in LB broth and were then washed, resuspended and cultured overnight at 30°C in CAA medium. Afterwards, bacteria were washed and again grown in CAA medium in the presence of 10 µM of ALBO in order to induce the expression of the corresponding iron uptake pathways. The bacteria were then used for ^{55}Fe uptake kinetics as described previously (23). The experiments were repeated with cells pretreated with 200 µM CCCP. This compound inhibits the protonmotive force across the bacterial cell membrane, thereby inhibiting TonB-dependent iron uptake (33).

Infection assay. A549 (ATCC® CCL-185™) human pulmonary epithelial cells were routinely cultivated at 37 °C, 5 % CO_2 in RPMI 1640 medium (Gibco) supplemented with 10 %

vol/vol FBS (Gibco) and passaged every 3 to 4 days as described previously (16). A549 cell viability was estimated using the Real Time-Glo™ MT cell viability assay kit (Promega™) as we described previously for equivalent infection conditions using *P. aeruginosa* (16).

A549 cells infections were also carried out as we described previously (16). The epithelial cells were seeded at a density of 1 x 10^6 cell per plate in 10 cm tissue culture dishes (Corning), one day before infection with *P. aeruginosa* PAO1 cells. *P. aeruginosa* was grown overnight in LB medium at 30°C under shaking, before being diluted to an $OD_{600\ nm}$ of 0.1 and incubated for 2 h 30, until the $OD_{600\ nm}$ of the suspension reached 0.4 to 0.6 indicating that bacteria are in exponential phase of growth. A549 cells were infected with a volume of this *P. aeruginosa* suspension equivalent to 50 x 10^6 CFU (multiplicity of infection of 50). FERRI, ALBO, ENT, TCV or TCVL6 were added to the A549 cells at the same moment as *P. aeruginosa* cells. The infection was allowed to carry on for 3 h at 37°C, 5 % CO_2. Afterwards, the plates were washed with cold PBS 1X buffer and the A549 cells and bacteria still adhering to the bottom of the plate harvested with a cell scraper. A549 cell and bacteria were then harvested by centrifugation and the dry pellet was re-suspended in one volume of PBS 1X buffer and stored at -80°C for proteomic analyses. For RT-qPCR analyses two volumes of RNAprotect Bacteria Reagent (Qiagen) were added before centrifugation and storage at -80°C overnight.

Quantitative real-time PCR on bacteria infecting epithelial cells. A549 cells were infected as described above. These analyses were carried out as previously described by our team (16). Samples were prepared as described above. On the day following sample preparation, lysis of the sample was carried out using Tris-EDTA pH 8 buffer containing 15 $mg.mL^{-1}$ lyzozyme, the lysates were homogenized using the QIAshredder kit (Qiagen) and RNA was extracted using RNeasy Mini kit (Qiagen). Genomic DNA digestion was performed with

DNase (RNase-Free DNase Set, Qiagen) and purified with a RNeasy Mini Elute cleanup kit (Qiagen). In order to assess for homogeneity of the amount of A549 cell RNA present in each sample, a quantification of GAPDH was used as a control. 1 µg of total RNA was then reverse-transcribed with a High-Capacity RNA-to-cDNA Kit, in accordance with the manufacturer's instructions (Applied Biosystems). The amounts of specific cDNAs were assessed in a StepOne Plus instrument (Applied Biosystems) with Power Sybr Green PCR Master Mix (Applied Biosystems) and the appropriate primers (Table 2SM), with the *uvrD* mRNA used as an internal control. The transcript levels for a given gene in a given strain were normalized with respect to those for *uvrD* and are expressed as a base two logarithm of the ratio (fold-change) relative to the reference conditions.

***Label-free proteomic analysis on bacteria infecting epithelial cells*.** A549 cells were infected as described above. The pellets of A549 cells and bacteria (five independent biological replicates) in PBS were diluted in Laemmli buffer before undergoing lysis as previously described (16). Proteins in lysate were cast into a 7.5 % acrylamide tube-gel as described (52) and digested with a 1:25 enzyme /protein ratio for 14h at 37°C. The resulting peptides were submitted to nanoLC-MS/MS analyses (750 ng injected) on a nanoACQUITY Ultra-Performance-LC systems hyphenated to a Q-Exactive Plus mass spectrometer as previously described (16).

The raw data obtained were converted into ".mfg" files with MSConvert software (ProteomeWizard, version 3.0.6090). Peaks were assigned with Mascot (Matrix Science, version 2.6.2) against an in-house database containing human entries from SwissProt database (17 March 2017, 20194 entries) and *P. aeruginosa* PAO1 entries from UniProtKB database (17 March 2017, 5677 entries). Common contaminant proteins such as human

keratins and trypsin were added to the database and concatenated with the reverse copies of all sequences. Trypsin was selected as enzyme, one missed cleavage was allowed. Database searches parameters in Mascot search engine and generated PSM validation were performed as previously described (16). For quantification purpose, the ".raw" files were converted into ".mzDB" files with MS Angel software (version 1.6.2). XIC quantification was performed in Proline software (53) using 5 ppm as m/z tolerance for the peptides abundance extraction. Loess smoothing was performed for the LC-MS runs alignments. Cross assignments of peptide ions were performed using 5 ppm as m/z tolerance and 60 s as retention time tolerance. Only proteins identified with at least one unique peptide were considered and only specific peptides were kept for the sum of protein abundances. The contaminants were excluded from the protein list prior to statistical analysis.

Experimental design and Statistical Rationale: Statistical analysis was performed using the ProStaR software (version 1.16.6) (54). Proteins identified in at least 4 replicates per condition were considered, normalization was performed using median quantile centering mode for all conditions. Imputation was performed at the protein level SLSA mode for partial observed values per condition and DetQuantile (2.5 %, factor 1) mode for values missing in entire condition. Welch's T-test was used to identify statistically differentially expressed proteins between two conditions. For each comparison, the p-value calibration was performed using the Benjamini-Hochberg procedure. Proteins with p-value below 0.001 were considered as differentially expressed, corresponding to a FDR between 1-5 %. Following values were obtained: 2.35% FDR for ENT, 2.26 % FDR for TCV, 7.33 % FDR for TCVL6, 0.72 % FDR for ALBO and 4.24% for FERRI.

The MS data were deposited to the ProteomeXchange Consortium via the PRIDE partner repository (55) with the PXD020378. Reviewer account details: **Usernam:** reviewer98509@ebi.ac.uk **Password:** . 3lVkMvDs.

Growth and quantification of mCHERRY fluorescence intensity. *P. aeruginosa* PAO1 strain were first grown overnight at 30°C in LB broth and were then washed, resuspended and cultured overnight at 30°C in iron-deficient CAA medium. Afterwards, bacteria were washed and again grown in CAA medium in 96-well plate (Greiner, U-bottomed microplate) in the presence or absence of 10 µM of ENT or TCV. The plate was incubated at 30 °C, with shaking, in a Tecan microplate reader (Infinite M200, Tecan) for measurements of $OD_{600\ nm}$ and mCherry (excitation/emission wavelengths: 570 nm/610 nm) fluorescence, at 30 min intervals, for 11 days. Every 24 h, the bacteria were centrifuged and resuspended in new CAA media with or without 10 µM ENT or TCV. We calculated the mean of three replicates for each measurement.

Acknowledgments

This work was partially funded by the *Centre National de la Recherche Scientifique* and grants from the associations Vaincre la Mucoviscidose and Association Gregory Lemarchal. In addition, these results were generated as part of the work of the Translocation Consortium (www.translocation.com), supported by the Innovative Medicines Joint Undertaking under Grant Agreement no. 115525, through financial contributions from the European Union's Seventh Framework Program (FP7/2007-2013) and contributions in kind from EFPIA companies. The equipment at the IPHC was partly funded by the French Proteomics Infrastructure (ProFI; ANR-10-INSB-08-03).

Author contributions

QP and PC performed all proteomic experiments

QP, PC and LS analyzed the proteomic data

QP also performed all the qRT-PCR, growth and ^{55}Fe uptake assays and wrote the paper

MM, FH and NZ performed the synthesis of TCV and TCVL6

VG performed the molecular biology and the experiments with PfeE mCherry

GLAM designed the syntheses of TCV and TCVL6

LS and IJS, secured funding, directed project, analyzed data and wrote paper

References

1. Tillotson GS. 2016. Trojan Horse Antibiotics-A Novel Way to Circumvent Gram-Negative Bacterial Resistance? Infect Dis (Auckl) 9:45–52.
2. Hider RC, Kong X. 2011. Chemistry and biology of siderophores. Natural product reports 27:637–57.
3. Schalk IJ, Mislin GLA, Brillet K. 2012. Structure, function and binding selectivity and stereoselectivity of siderophore-iron outer membrane transporters. Curr Top Membr 69:37–66.
4. Mislin GLA, Schalk IJ. 2014. Siderophore-dependent iron uptake systems as gates for antibiotic Trojan horse strategies against *Pseudomonas aeruginosa*. Metallomics 6:408–420.
5. Górska A, Sloderbach A, Marszałł MP. 2014. Siderophore-drug complexes: potential medicinal applications of the “Trojan horse” strategy. Trends Pharmacol Sci 35:442–449.
6. Zhanel GG, Golden AR, Zelenitsky S, Wiebe K, Lawrence CK, Adam HJ, Idowu T, Domalaon R, Schweizer F, Zhanel MA, Lagacé-Wiens PRS, Walkty AJ, Noreddin A, Lynch Iii JP, Karlowsky JA. 2019. Cefiderocol: A siderophore cephalosporin with activity against carbapenem-resistant and multidrug-Resistant Gram-negative Bacilli. Drugs 79:271–289.
7. Gause GF. 1955. Recent studies on albomycin, a new antibiotic. Br Med J 2:1177–1179.
8. Benz G, Schroeder T, Kurz J, Wuensche C, Karl W, G. S, Pfitzner J, Schmidt D. 1982. Konstitution der Desferriform der Albomycine δ1, δ2, ε. Angew Chem 21:1322–1335.
9. Sackmann W, Reusser P, Neipp L, Kradolfer F, Gross F. 1962. Ferrimycin A, a new iron-containing antibiotic. Antibiot Chemother (Northfield) 12:34–45.
10. Selzer GB. 1980. Antibiotics: Isolation, separation, and purification. Edited by Marvin J. Weinstein and Gerald H. Wagman. (Journal of Chromatography Library, Vol. 15.)

581 Elsevier/North-Holland Inc., 52 Vanderbilt Ave., New York, NY 10017. 1978. 769 pp. 16 ×
582 24 cm. Price $84.75. Journal of Pharmaceutical Sciences 69:754–754.
583 11. Vertesy L, Aretz W, Fehlhaber H-W, Kogler H. 1995. Salmycins A-D, antibiotics from
584 *Streptomyces violaceus* DSM 8286 having a siderophore -aminoglycoside structure.
585 Helvetica Chimica Acta 78:46–60.
586 12. Cornelis P, Dingemans J. 2013. *Pseudomonas aeruginosa* adapts its iron uptake strategies
587 in function of the type of infections. Frontiers in cellular and infection microbiology 3:75.
588 13. Poole K, Young L, Neshat S. 1990. Enterobactin-mediated iron transport in *Pseudomonas*
589 *aeruginosa*. J Bacteriol 172:6991–6.
590 14. Hannauer M, Barda Y, Mislin GL, Shanzer A, Schalk IJ. 2010. The ferrichrome uptake
591 pathway in *Pseudomonas aeruginosa* involves an iron release mechanism with acylation
592 of the siderophore and a recycling of the modified desferrichrome. J Bacteriol 192:1212–
593 20.
594 15. Barber MF, Elde NC. 2015. Buried treasure: evolutionary perspectives on microbial iron
595 piracy. Trends Genet 31:627–636.
596 16. Perraud Q, Cantero P, Roche B, Gasser V, Normant VP, Kuhn L, Hammann P, Mislin GLA,
597 Ehret-Sabatier L, Schalk IJ. 2020. Phenotypic adaption of *Pseudomonas aeruginosa* by
598 hacking siderophores produced by other microorganisms. Mol Cell Proteomics 19:589–
599 607.
600 17. Schalk IJ, Guillon L. 2013. Fate of ferrisiderophores after import across bacterial outer
601 membranes: different iron release strategies are observed in the cytoplasm or periplasm
602 depending on the siderophore pathways. Amino Acids 44:1267–1277.

18. Dean CR, Neshat S, Poole K. 1996. PfeR, an enterobactin-responsive activator of ferric enterobactin receptor gene expression in *Pseudomonas aeruginosa*. J Bacteriol 178:5361–5369.

19. Visca P, Leoni L, Wilson MJ, Lamont IL. 2002. Iron transport and regulation, cell signalling and genomics: lessons from *Escherichia coli* and *Pseudomonas*. Mol Microbiol 45:1177–90.

20. Michel L, Gonzalez N, Jagdeep S, Nguyen-Ngoc T, Reimmann C. 2005. PchR-box recognition by the AraC-type regulator PchR of *Pseudomonas aeruginosa* requires the siderophore pyochelin as an effector. Molecular microbiology 58:495–509.

21. Llamas MA, Sparrius M, Kloet R, Jimenez CR, Vandenbroucke-Grauls C, Bitter W. 2006. The heterologous siderophores ferrioxamine B and ferrichrome activate signaling pathways in *Pseudomonas aeruginosa*. Journal of bacteriology 188:1882–91.

22. Llamas MA, Imperi F, Visca P, Lamont IL. 2014. Cell-surface signaling in Pseudomonas: stress responses, iron transport, and pathogenicity. FEMS microbiology reviews 38:569–97.

23. Gasser V, Baco E, Cunrath O, August PS, Perraud Q, Zill N, Schleberger C, Schmidt A, Paulen A, Bumann D, Mislin GLA, Schalk IJ. 2016. Catechol siderophores repress the pyochelin pathway and activate the enterobactin pathway in *Pseudomonas aeruginosa*: an opportunity for siderophore-antibiotic conjugates development. Environ Microbiol 18:819–832.

24. Perraud Q, Cantero, Paola P, Roche B, Gasser V, Normant V, Kuhn L, Hammann P, Mislin GLA, Ehret-Sabatier L, Schalk IJ. Phenotypic adaption of *Pseudomonas aeruginosa* by hacking siderophores produced by other microorganisms. Molecular and Cellular Proteomic.

627 25. Braun V, Pramanik A, Gwinner T, Koberle M, Bohn E. 2009. Sideromycins: tools and
628 antibiotics. Biometals : an international journal on the role of metal ions in biology,
629 biochemistry, and medicine 22:3–13.
630 26. Wencewicz TA, Mollmann U, Long TE, Miller MJ. 2009. Is drug release necessary for
631 antimicrobial activity of siderophore-drug conjugates? Syntheses and biological studies
632 of the naturally occurring salmycin "Trojan Horse" antibiotics and synthetic
633 desferridanoxamine-antibiotic conjugates. Biometals 22:633–48.
634 27. Albrecht-Gary AM, Blanc S, Rochel N, Ocacktan AZ, Abdallah MA. 1994. Bacterial iron
635 transport: coordination properties of pyoverdin PaA, a peptidic siderophore of
636 *Pseudomonas aeruginosa*. Inorg Chem 33:6391–6402.
637 28. Brandel J, Humbert N, Elhabiri M, Schalk IJ, Mislin GLA, Albrecht-Garry A-M. 2012.
638 Pyochelin, a siderophore of *Pseudomonas aeruginosa*: Physicochemical characterization
639 of the iron(III), copper(II) and zinc(II) complexes. Dalton Trans 41:2820–34.
640 29. Folschweiller N, Gallay J, Vincent M, Abdallah MA, Pattus F, Schalk IJ. 2002. The
641 interaction between pyoverdin and its outer membrane receptor in *Pseudomonas*
642 *aeruginosa* leads to different conformers: a time-resolved fluorescence study.
643 Biochemistry 41:14591–601.
644 30. Loomis L, Raymond KN. 1991. Solution equilibria of enterobactin complexes. Inorg Chem
645 30:906–911.
646 31. Anderegg G, L'Eplattenier F, Schwarzenbach G. 1963. Hydroxamatkomplexe III. Eisen(III)-
647 Austausch zwischen Sideraminen und Komplexonen. Diskussion der Bildungskonstanten
648 der Hydroxamatkomplexe. Helvetica Chimica Acta 46:1409–1422.
649 32. Normant VP, Josts I, Kuhn L, Perraud Q, Fritsch S, Hammann P, Mislin GLA, Tidow H,
650 Schalk IJ. 2020. Nocardamine-dependent iron uptake in *Pseudomonas aeruginosa:*

exclusive involvement of the FoxA outer membrane transporter. submitted to ACS Chem Biol.

33. Clément E, Mesini PJ, Pattus F, Abdallah MA, Schalk IJ. 2004. The binding mechanism of pyoverdin with the outer membrane receptor FpvA in *Pseudomonas aeruginosa* is dependent on its iron-loaded status. Biochemistry 43:7954–65.

34. Postle K, Larsen RA. 2007. TonB-dependent energy transduction between outer and cytoplasmic membranes. Biometals 20:453–65.

35. Celia H, Noinaj N, Buchanan SK. 2020. Structure and Stoichiometry of the Ton Molecular Motor. Int J Mol Sci 21.

36. Pollack M. 1983. The role of exotoxin A in Pseudomonas disease and immunity. Rev Infect Dis 5 Suppl 5:S979-984.

37. Chaudry GJ, Holmans PL, Clowes RC, Draper RK. 1992. *Pseudomonas aeruginosa* exotoxin A. Targeted Diagn Ther 7:405–423.

38. Thibodeaux BA, Caballero AR, Dajcs JJ, Marquart ME, Engel LS, O'Callaghan RJ. 2005. *Pseudomonas aeruginosa* protease IV: a corneal virulence factor of low immunogenicity. Ocul Immunol Inflamm 13:169–182.

39. Oh J, Li X-H, Kim S-K, Lee J-H. 2017. Post-secretional activation of Protease IV by quorum sensing in *Pseudomonas aeruginosa*. Scientific Reports 7:1–10.

40. Laarman AJ, Bardoel BW, Ruyken M, Fernie J, Milder FJ, van Strijp JAG, Rooijakkers SHM. 2012. *Pseudomonas aeruginosa* alkaline protease blocks complement activation via the classical and lectin pathways. J Immunol 188:386–393.

41. Muriel C, Arrebola E, Redondo-Nieto M, Martínez-Granero F, Jalvo B, Pfeilmeier S, Blanco-Romero E, Baena I, Malone JG, Rivilla R, Martín M. 2018. AmrZ is a major determinant of c-di-GMP levels in *Pseudomonas fluorescens* F113. Sci Rep 8:1979.

42. Mavrodi DV, Bonsall RF, Delaney SM, Soule MJ, Phillips G, Thomashow LS. 2001. Functional analysis of genes for biosynthesis of pyocyanin and phenazine-1-carboxamide from *Pseudomonas aeruginosa* PAO1. J Bacteriol 183:6454–6465.

43. Recinos DA, Sekedat MD, Hernandez A, Cohen TS, Sakhtah H, Prince AS, Price-Whelan A, Dietrich LEP. 2012. Redundant phenazine operons in *Pseudomonas aeruginosa* exhibit environment-dependent expression and differential roles in pathogenicity. Proc Natl Acad Sci USA 109:19420–19425.

44. Duong F, Bonnet E, Géli V, Lazdunski A, Murgier M, Filloux A. 2001. The AprX protein of *Pseudomonas aeruginosa*: a new substrate for the Apr type I secretion system. Gene 262:147–153.

45. Wilderman PJ, Vasil AI, Johnson Z, Wilson MJ, Cunliffe HE, Lamont IL, Vasil ML. 2001. Characterization of an endoprotease (PrpL) encoded by a PvdS-regulated gene in *Pseudomonas aeruginosa*. Infect Immun 69:5385–5394.

46. Casilag F, Lorenz A, Krueger J, Klawonn F, Weiss S, Häussler S. 2016. The LasB elastase of *Pseudomonas aeruginosa* acts in concert with alkaline protease AprA to prevent flagellin-mediated immune recognition. Infect Immun 84:162–171.

47. Yahr TL, Vallis AJ, Hancock MK, Barbieri JT, Frank DW. 1998. ExoY, an adenylate cyclase secreted by the *Pseudomonas aeruginosa* type III system. Proc Natl Acad Sci USA 95:13899–13904.

48. Wolz C, Hellstern E, Haug M, Galloway DR, Vasil ML, Döring G. 1991. *Pseudomonas aeruginosa* LasB mutant constructed by insertional mutagenesis reveals elastolytic activity due to alkaline proteinase and the LasA fragment. Mol Microbiol 5:2125–2131.

49. Perraud Q, Moynié L, Gasser V, Munier M, Godet J, Hoegy F, Mély Y, Mislin GLA, Naismith JH, Schalk IJ. 2018. A key role for the periplasmic PfeE esterase in iron acquisition via the siderophore enterobactin in *Pseudomonas aeruginosa*. ACS Chem Biol 13:2603–2614.
50. Demange P, Wendenbaum S, Linget C, Mertz C, Cung MT, Dell A Abdallah, MA. 1990. Bacterial siderophores: structure and NMR assigment of pyoverdins PaA, siderophores of *Pseudomonas aeruginosa* ATCC 15692. Biol Metals 3:155–170.
51. Baco E, Hoegy F, Schalk IJ, Mislin GL. 2014. Diphenyl-benzo[1,3]dioxole-4-carboxylic acid pentafluorophenyl ester: a convenient catechol precursor in the synthesis of siderophore vectors suitable for antibiotic Trojan horse strategies. Organic & biomolecular chemistry 12:749–57.
52. Muller L, Fornecker L, Van Dorsselaer A, Cianférani S, Carapito C. 2016. Benchmarking sample preparation/digestion protocols reveals tube-gel being a fast and repeatable method for quantitative proteomics. Proteomics 16:2953–2961.
53. Bouyssié D, Hesse A-M, Mouton-Barbosa E, Rompais M, Macron C, Carapito C, Gonzalez de Peredo A, Couté Y, Dupierris V, Burel A, Menetrey J-P, Kalaitzakis A, Poisat J, Romdhani A, Burlet-Schiltz O, Cianférani S, Garin J, Bruley C. 2020. Proline: an efficient and user-friendly software suite for large-scale proteomics. Bioinformatics 36:3148–3155.
54. Wieczorek S, Combes F, Lazar C, Giai Gianetto Q, Gatto L, Dorffer A, Hesse A-M, Couté Y, Ferro M, Bruley C, Burger T. 2017. DAPAR & ProStaR: software to perform statistical analyses in quantitative discovery proteomics. Bioinformatics 33:135–136.
55. Vizcaíno JA, Deutsch EW, Wang R, Csordas A, Reisinger F, Ríos D, Dianes JA, Sun Z, Farrah T, Bandeira N, Binz P-A, Xenarios I, Eisenacher M, Mayer G, Gatto L, Campos A, Chalkley RJ, Kraus H-J, Albar JP, Martinez-Bartolomé S, Apweiler R, Omenn GS, Martens L, Jones

AR, Hermjakob H. 2014. ProteomeXchange provides globally coordinated proteomics data submission and dissemination. Nat Biotechnol 32:223–226.

56. Yahr TL, Vallis AJ, Hancock MK, Barbieri JT, Frank DW. 1998. ExoY, an adenylate cyclase secreted by the *Pseudomonas aeruginosa* type III system. Proc Natl Acad Sci USA 95:13899–13904.

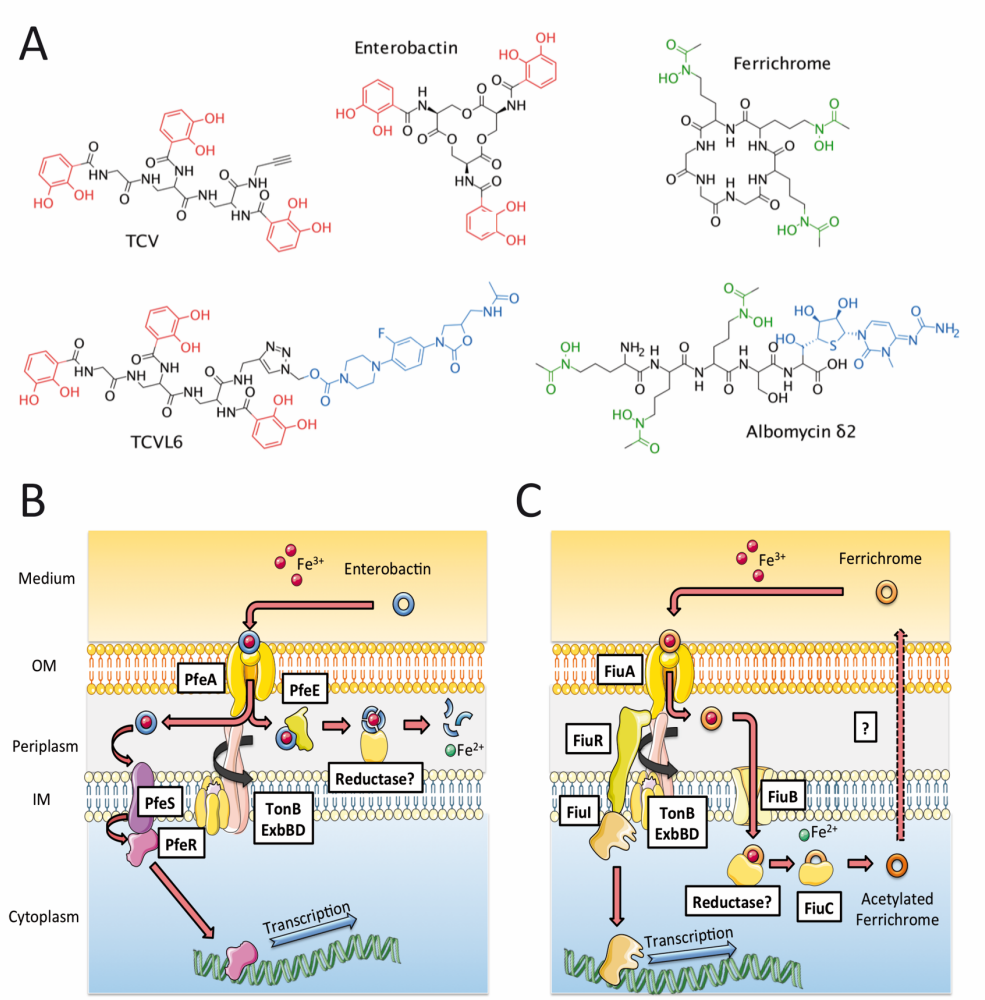

727

728 **Fig 1. A. Structure of ferrichrome (FERRI), albomycin (ALBO), enterobactin (ENT), tris-**
729 **catechol vector (TCV), and tris-catechol-linezolid vector (TCVL6). B and C. ENT- and FERRI-**
730 **dependent iron-uptake pathways in *P. aeruginosa*, respectively.** FERRI and ENT loaded with
731 iron are recognized at the bacterial surface by the OMTs FiuA and PfeA, respectively, and
732 transported across the outer membrane. Iron release from ENT occurs in the bacterial
733 periplasm and involves hydrolysis of the siderophore by the esterase PfeE and an iron-
734 reduction step by a non-identified reductase. ENT-Fe does not enter the bacterial cytoplasm
735 in *P. aeruginosa* cells. Concerning FERRI-Fe, once in the bacterial periplasm, the complex is
736 transported further across the inner membrane by the protonmotive-dependent permease
737 FiuB and iron is released from FERRI in the bacterial cytoplasm by a mechanism involving
738 acetylation of the siderophore by FiuC and iron reduction by an unknown reductase (14).
739

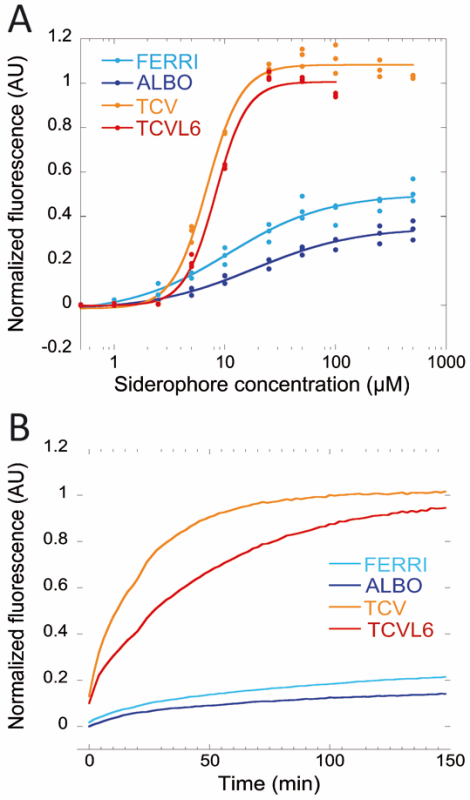

740

741

742 **Fig 2. A. Ability of FERRI, ALBO, TCV, and TCVL6 to scavenge iron from PVD-Fe complexes.**
743 Ten micromoles of PVD-Fe in 100 mM HEPES pH 7.4 was incubated with increasing
744 concentrations of FERRI, ALBO, TCV, or TCVL6 for 48 h (until equilibrium was reached), as
745 described previously (16). Metal-free PVD is fluorescent, with absorbance typically at 447 nm,
746 and PVD-Fe is not (27, 29). Apo PVD formation was thus followed by monitoring its fluorescent
747 at 447 nm (excitation at 400 nm). The data were normalized using the formula $(F_{MEASURED} -$
748 $F_{PVD\text{-}Fe})/(F_{PVD} - F_{PVD\text{-}Fe})$, $F_{MEASURED}$ being the fluorescence measured for each experimental
749 condition, $F_{PVD\text{-}Fe}$ the fluorescence of 10 µM PVD-Fe, and F_{PVD} the fluorescence of 10 µM PVD.
750 **B. Kinetics of PVD-Fe dissociation in the presence of FERRI, ALBO, TCV, or TCVL6.** Ten
751 micromoles of PVD-Fe in 100 mM HEPES buffer pH 7.4 was incubated with 100 µM FERRI,
752 ALBO, TCV, or TCVL6, as described in Materials and Methods. The kinetics of apo PVD
753 formation were followed by monitoring the fluorescence emission at 447 nm (excitation at
754 400 nm), as previously described (16).

755

756

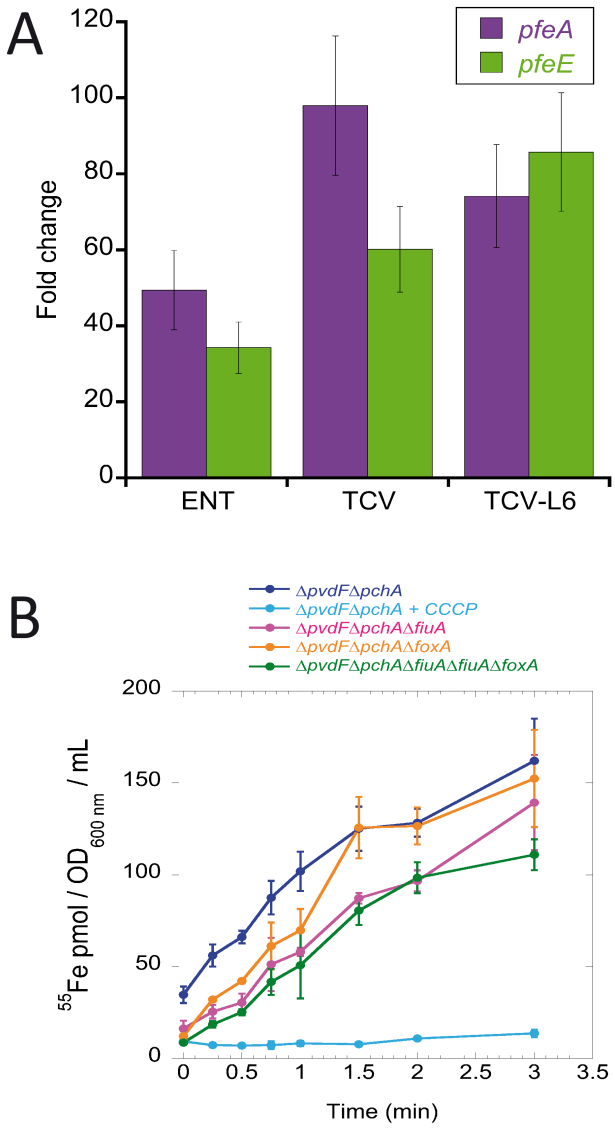

757

758 **Fig 3. A. Analysis of changes in the transcription of the *pfeA* and *pfeE* genes.** RT-qPCR was
759 performed on RNA from *P. aeruginosa* PAO1 cells grown in CAA medium, with or without
760 supplementation with 10 µM ENT, TCV, or TCVL6 conjugate. The data are normalized relative
761 to the reference gene *uvrD* and are representative of three independent experiments
762 performed in triplicate (*n* =3). *pfeA* encodes the OMT of ENT and *pfeE* the esterase involved
763 in ENT hydrolysis.

764 **B. ^{55}Fe uptake in *P. aeruginosa* strains using ALBO as a siderophore.** Δ*pvdF*Δ*pchA* and
765 Δ*pvdF*Δ*pchA*Δ*fiuA* cells grown in iron-restricted CAA medium, in the presence of 10 µM ALBO
766 to induce any needed OMT, were incubated with 500 nM ALBO-^{55}Fe and the kinetics of ^{55}Fe
767 uptake measured as previously described (23). As a control, the experiment was repeated in
768 the presence of 200 µM CCCP protonophore for Δ*pvdF*Δ*pchA* cells. Errors bars were calculated
769 from three independent biological replicates.

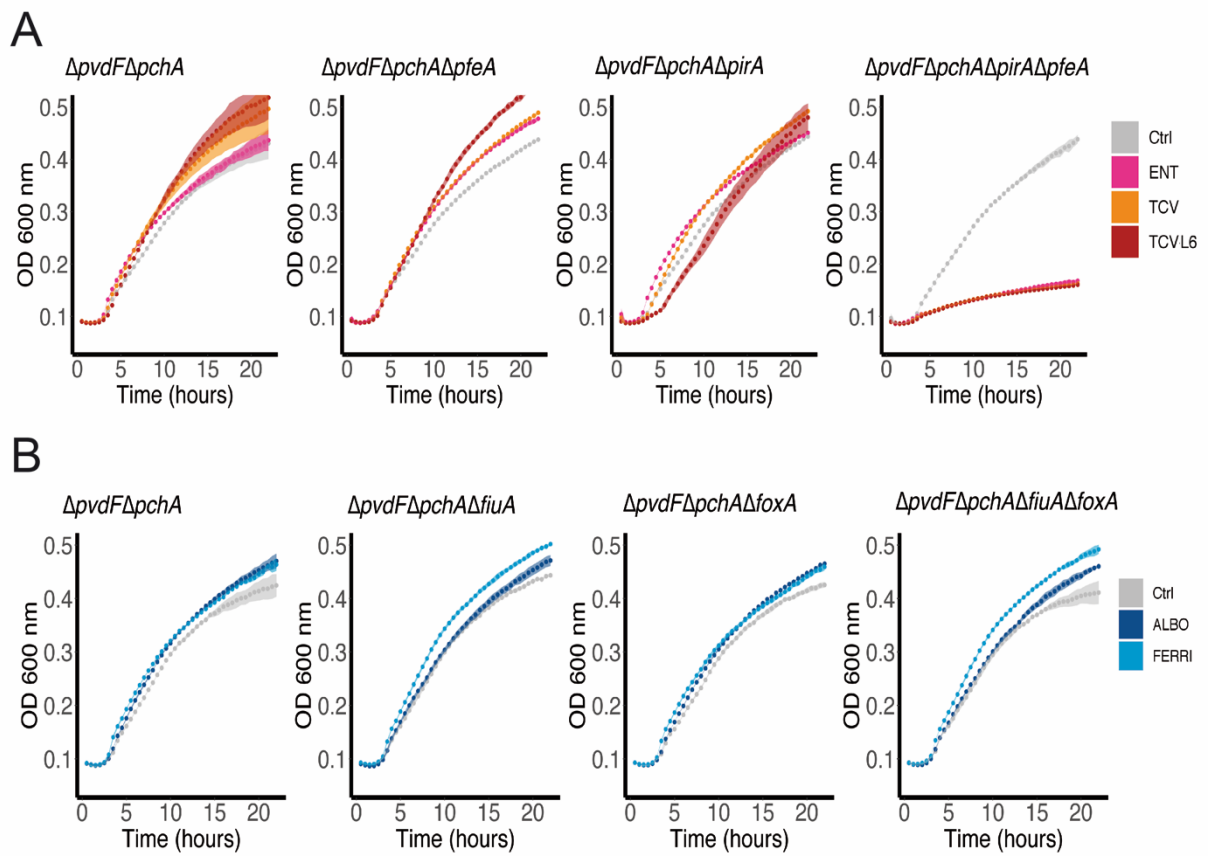

770

771

772 **Fig 4. Bacterial growth in the presence of FERRI, ALBO, ENT, TCV, or TCVL6.** Various strains
773 (Δ*pvdF*Δ*pchA* and its corresponding *pfeA*, *pirA*, *fiuA* and *foxA* deletion mutants) were grown
774 in iron-restricted CAA medium, with or without 10 µM FERRI, ALBO, ENT, TCV, or TCVL6, at
775 37°C. The growth curves are the mean of three independent biological triplicates.

776

777

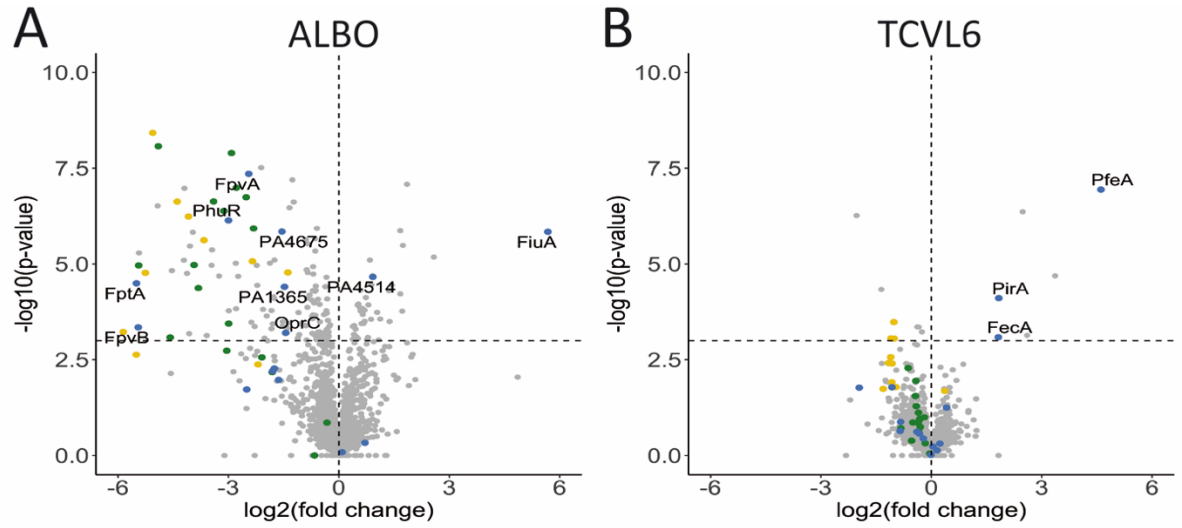

C

	FERRI		ALBO		ENT		TCV		TCVL6	
PA4156	0.13	ns		nd		nd		nd		nd
FecA	-0.42	ns	0.71	ns	-0.80	ns	2.15	***	1.82	***
FemA	1.32	ns		nd		nd		nd		nd
FiuA	5.36	***	5.68	***		nd		nd		nd
FoxA	-0.99	ns		nd		nd		nd		nd
FptA	-2.46	***	-5.50	***	-4.09	***	-2.70	***	-1.07	*
FpvA	-0.71	***	-2.45	***	-1.19	***	-0.84	***	0.05	ns
FpvB	0.13	ns	-5.45	***	0.06	ns	-0.03	ns	-0.39	ns
HasR	-0.13	ns	0.09	ns	-3.19	***	-1.22	*	-0.85	ns
OprC	-0.59	**	-1.44	***	-0.81	ns	-1.56	**	-1.96	*
PA0151	0.07	ns		nd	-0.56	*	0.14	ns	0.41	ns
PA0434	-0.59	ns		nd		nd		nd		nd
PA0781	-0.82	ns		nd		nd		nd		nd
PA1302	0.18	ns	-1.64	*	0.33	ns	-0.37	ns	-0.22	ns
PA1365	0.02	ns	-1.47	***	-0.16	ns	0.37	ns	0.15	ns
PA3268	0.06	ns	-1.80	**	0.26	ns	-0.07	ns	-0.84	ns
PiuA	0.17	ns	0.92	***	0.71	*	1.36	***	0.23	ns
PA4675	-0.06	ns	-1.55	***	0.04	ns	0.36	**	-0.32	ns
PfeA	-0.19	ns	-1.75	**	3.44	***	4.77	***	4.61	***
PhuR	-0.15	ns	-3.00	***	-0.37	*	-0.12	ns	-0.01	ns
PirA	-0.16	ns	-2.50	*	0.70	*	1.70	***	1.83	***

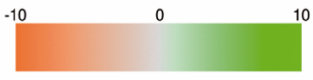

D

	FERRI		ALBO		ENT		TCV		TCVL6	
FptA	-2.46	***	-5.50	***	-4.09	***	-2.70	***	-1.07	*
PchA	-2.63	***	-3.67	***	-3.80	***	-3.12	***	-1.02	***
PchB	-2.99	***	-5.06	***	-5.10	***	-3.49	***	-1.31	*
PchC	-2.36	***	-4.08	***	-3.22	***	-2.10	***	-0.96	*
PchD	-2.84	***	-5.26	***	-4.47	**	-2.73	***	-1.07	*
PchE	-3.14	***	-5.50	**	-4.88	***	-3.11	***	-1.17	**
PchF	-2.60	***	-2.35	***	-4.00	***	-2.74	***	-1.01	***
PchG	-3.66	**	-5.86	***	-2.80	***	-2.54	***	-1.10	**
PchH	-2.90	***	-2.20	**	-5.73	**	-4.03	**	-1.10	***
PchI	-5.33	***	-1.38	***	-5.56	***	-4.53	**	-1.07	**
PchR	0.17	ns	-4.39	***	0.45	*	0.35	*	0.36	*

E

	FERRI		ALBO		ENT		TCV		TCVL6	
FpvA	-0.71	***	-2.45	***	-1.19	***	-0.84	***	0.05	ns
FpvC	-0.41	ns	-2.09	**	-1.67	**	-0.99	*	-0.54	ns
FpvF	-0.52	***	-2.32	***	-1.24	***	-0.83	**	-0.35	ns
FpvH	-0.66	ns	-0.66	ns		nd		nd		nd
FpvK	-0.32	ns	-0.32	ns		nd		nd		nd
OpmQ	-0.42	*	-1.81	**	-1.30	***	-1.08	***	-0.19	ns
PvdA	-0.52	***	-3.68	***	-1.35	***	-1.28	***	-0.42	*
PvdD	-0.51	***	-2.99	***	-1.34	***	-1.31	***	-0.36	ns
PvdE	-0.51	**	-3.93	***	-1.48	***	-1.21	***	-0.50	ns
PvdF	-0.46	*	-3.12	***	-1.24	***	-0.84	**	-0.16	ns
PvdH	-0.53	***	-4.90	***	-1.74	***	-1.65	***	-0.63	**
PvdJ	-0.53	***	-2.92	***	-1.33	***	-1.14	***	-0.30	ns
PvdJ	-0.44	***	-2.52	***	-1.19	***	-1.20	***	-0.32	ns
PvdL	-0.57	***	-3.41	***	-1.49	***	-1.36	***	-0.43	*
PvdN	-0.52	***	-3.82	***	-1.32	***	-1.15	***	-0.35	ns
PvdO	-0.39	ns	-4.58	***	-1.22	**	-0.95	**	-0.04	ns
PvdP	-0.52	***	-5.44	***	-1.44	***	-1.30	***	-0.83	ns
PvdQ	-0.52	***	-3.04	**	-1.30	***	-1.05	***	-0.31	ns
PvdR	-0.42	**	-2.78	***	-1.17	**	-1.80	**	-0.41	ns

Fig 5. Analysis of changes in the expression of proteins involved in iron-uptake pathways in *P. aeruginosa* cells during A549 epithelial cell infection, in the presence or absence of ALBO, TCVL6, FERRI, ENT or TCV. A-B. Proteomic analyses were performed on *P. aeruginosa* PAO1

cells after a 3-h infection of A549 epithelial cells in RPMI medium, in the presence or absence of 10 µM ALBO or TCVL6. Median values measured in the infection assay supplemented with either 10 µM ALBO or TCVL6 were plotted against those measured in the infection assay in the absence of supplementation with siderophore-antibiotic compounds. The median values represent the median of the relative intensity of each protein normalized against all proteins detected by shotgun analysis (n = 5).

C-E. Heat maps of various proteins involved in the PVD (E) and PCH (D) pathways and of OMTs (C): the darker the shade of green, the higher the induced expression of the protein. Only the proteins for which a change in the level of expression was observed are shown. The nd note indicates that the protein hasn't been identified, ns indicates that the p-value is higher than 0.05; the *, ** and *** symbols indicates a p-value lower than 0.05, 0.01 and 0.001 respectively. All siderophore or siderophore-antibiotic compounds were added at 10 µm.

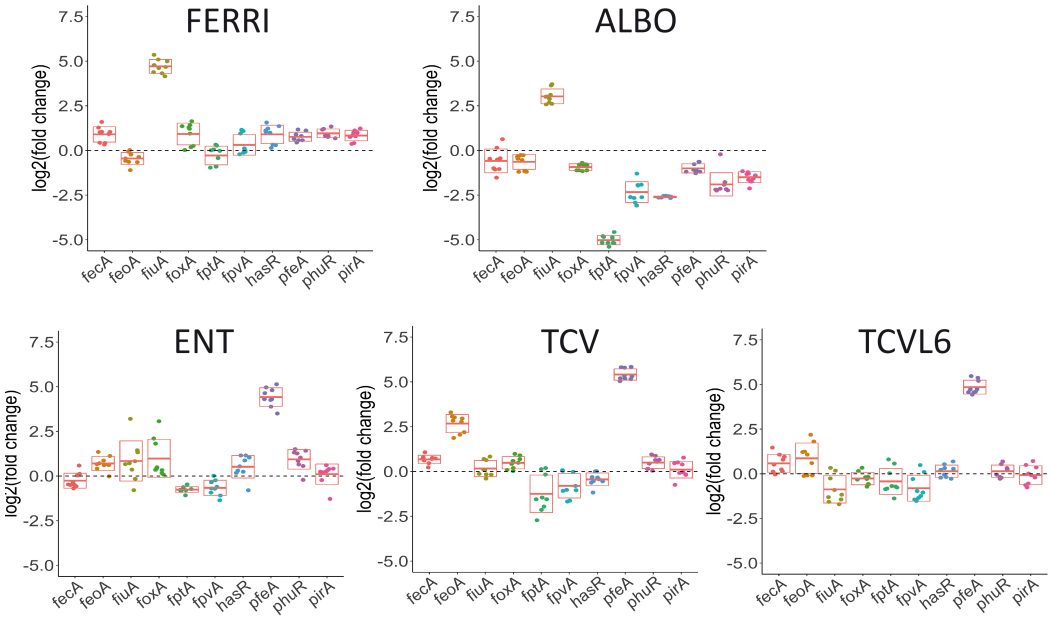

Fig 6. Analysis of changes in the transcription of genes involved in iron-uptake pathways in *P. aeruginosa* cells during A549 epithelial cell infection, in the presence or absence of FERRI, ALBO, ENT, TCV, or TCVL6. RT-qPCR analyses were performed, similar to the proteomic analyses, on *P. aeruginosa* PAO1 cells after a 3-h infection of A549 epithelial cells in RPMI medium, in the presence of absence of 10 µM FERRI, ALBO, ENT, TCV, or TCVL6. The data were normalized relative to the reference gene *uvrD* and are representative of three independent experiments, each performed in triplicate (n = 3). Results are given as the ratio between the values obtained in the presence of the siderophores or conjugates over those obtained in their absence. *fecA* encodes the OMT of ferri-citrate, *feoA*, the ferrous transporter, and *fiuA,* the OMT of FERRI, *foxA,* that of ferrioxamine B, *fptA,* that of PCH, *fpvA,* that of PVD, *hasR* and *phuR, that* of heme, *pfeA* and *pirA, that* of ENT and *piuA,* that of an unknown siderophore.

A

AlgC	-0.3	ns	-0.347	**	-0.165	ns	-0.75	ns	-0.256	ns
AlgP	-0.24	*	-0.84	ns	-0.14	ns	-0.147	ns	-0.154	ns
AlgQ		nd		nd	-0.439	**	-0.271	*	-0.122	ns
ChpA	-0.175	ns	-0.636	*	-0.191	ns	0.1	ns	-0.71	ns
CsrA	0.136	ns	0.376	*		nd		nd		nd
ExoS	-0.161	ns	-1.564	*	-0.56	**	-0.254	ns	0.12	ns
ExoT	-0.116	ns	-1.743	**	-0.145	ns	0.178	ns	0.9	ns
ExsA	-0.62	*	-3.59	***	-1.219	*	-0.455	ns	-0.373	ns
ExsD	-0.431	***	-2.217	***	-0.661	*	-0.416	***	-0.27	*
FabV	0.23	ns	0.276	**	0.429	***	0.26	**	-0.54	ns
FleQ	-0.32	ns	0.291	**	0.69	ns	0.12	ns	-0.63	ns
FliC	0.285	ns	-0.253	*	0.268	*	0.27	ns	-0.134	ns
FliF	-0.268	*		nd		nd		nd		nd
FliM	0.33	*	0.235	ns	0.92	ns	0.15	ns	0.84	ns
FliS	0.387	*	-1.758	*	0.169	ns	-0.152	ns	-0.245	ns
Fur	0.51	ns	0.118	*	-0.113	ns	-0.54	ns	0.119	ns
GalU	-0.4	ns	-0.217	*	-0.812	ns	0.51	ns	0.67	ns
GpmI	-0.115	ns	-0.522	**	-0.566	ns	-0.296	ns	-0.688	ns
Hcp1	0.231	ns	0.8	ns	-0.839	**	-0.198	ns	-0.37	*
HtpG	-0.228	*	-0.525	***	-0.283	ns	-0.153	ns	-0.525	ns
LasR	-0.59	ns	-0.726	***	-0.635	ns	-0.515	ns	-0.27	ns
Lon	-0.3	ns	-0.24	*	-0.182	*	-0.91	ns	-0.126	ns
MucA		nd		nd	-1.131	ns	-1.26	*	-0.611	ns
MucB		nd	1.96	*		nd		nd		nd
MucD	-0.214	ns	-0.713	***	-0.665	ns	-0.76	ns	-0.69	ns
NuoC	0.44	ns	0.656	*	0.598	*	0.32	ns	-0.518	ns
OpgG	-0.11	ns	-0.334	*	0.31	ns	-0.96	ns	-0.593	ns
OxyR	-0.229	ns	0.119	ns	0.215	*	-0.9	ns	-0.43	ns
PA0084	0.344	*		nd		nd		nd		nd
PA0151	0.73	ns		nd	-0.565	*	0.137	ns	0.415	ns
PA0423	-0.253	ns	-2.278	**	-1.252	**	-1.159	**	-0.861	ns
PA2393	-0.56	***	-2.41	**	-1.231	***	-1.393	***	-0.39	**
PA2462	0.55	ns	1.288	*		nd		nd		nd
PA2634	-0.344	**	-1.41	***	-0.791	**	-0.44	**	-0.187	ns
PA3649	0.16	ns	-0.661	*		nd		nd		nd
PA4491	-0.11	ns	-0.12	ns	-1.237	*	-0.487	ns	-0.453	*
PA5312	-0.46	ns	0.43	ns	-0.363	ns	-0.332	**	-0.645	ns
PA5441	-0.2	ns	-0.321	**	0.2	ns	-0.177	ns	-0.594	ns
PcrH	-0.218	**	-1.263	***	-0.362	*	-0.37	ns	0.14	ns
PcrV	0.117	ns	-1.833	***	-0.245	ns	-0.26	ns	-0.733	*
Pgk	-0.1	ns	0.42	ns	0.137	ns	0.25	*	-0.291	ns
PilE		nd		nd	-0.582	***	-0.292	ns	-0.21	ns
PilF	-0.172	*	-0.137	ns	0.19	ns	-0.51	ns	-0.99	ns
PilO	-0.149	*	-0.436	*	-0.811	*	-1.78	*	-1.246	*
PilQ	-0.57	ns	-0.337	***	-0.362	*	-0.184	ns	-0.412	ns
PilU	0.319	*	0.425	ns	-0.384	ns	-0.129	ns	0.53	ns
PopB	-0.452	ns	-4.67	***	-0.781	**	0.46	ns	0.552	ns
PopD	-0.27	*	-3.461	***	-0.38	ns	0.487	ns	0.31	ns
PopN	-0.373	ns	-4.197	***	-0.89	ns	-0.799	ns	-0.524	ns
PscB	0.352	ns	-0.983	*	-1.171	***	-0.196	ns	-0.83	ns
PscC	-0.896	ns	-2.793	***		nd		nd		nd
PscD	-0.194	ns	-3.449	***		nd		nd		nd
PscE		nd	-3.967	***		nd		nd		nd
PscF	-0.536	**	-4.47	***	-1.516	*	-0.583	*	-0.641	*
PscJ	-0.512	*	-2.99	***	-0.688	*	-0.373	ns	-0.48	ns
PurD	0.157	ns	0.144	ns	0.224	*	0.125	ns	-0.3	ns
TssC1		nd	0.126	ns	-0.512	*	-0.291	ns	-0.68	*
TssK1		nd	-0.278	ns	-0.462	*	-0.23	ns	-0.13	ns
TypA	0.7	ns	0.12	ns	0.348	**	0.142	ns	-0.177	ns
Vfr	0.32	ns	0.196	*	0.151	ns	0.24	ns	-0.217	ns
WbpA	0.16	ns	0.3	**	-0.19	ns	-0.18	ns	-0.225	ns
WbpB	-0.9	ns	0.255	*	0.29	ns	0.9	ns	-0.5	ns
WbpD	-0.374	*	-0.295	ns	0.255	ns	-0.162	ns	-0.25	ns
WbpE	0.23	ns	-0.228	*	-0.298	ns	0.47	ns	0.77	ns
WbpG	-0.292	*	-0.74	***	0.35	ns	-0.117	ns	-0.349	ns
WbpH	-0.185	*	-0.495	*	0.19	ns	0.15	ns	-0.298	ns
WbpI	0.32	ns	-0.736	***	0.66	ns	-0.62	ns	-0.229	ns
WbpJ	-0.157	ns	-0.628	***	-0.976	ns	-0.5	ns	-0.61	ns
WbpK	0.13	ns	-0.752	**	-0.6	ns	0.17	ns	-0.35	ns
Wzz	-0.86	ns	0.681	*	-0.736	*	-0.167	ns	-1.164	*

B

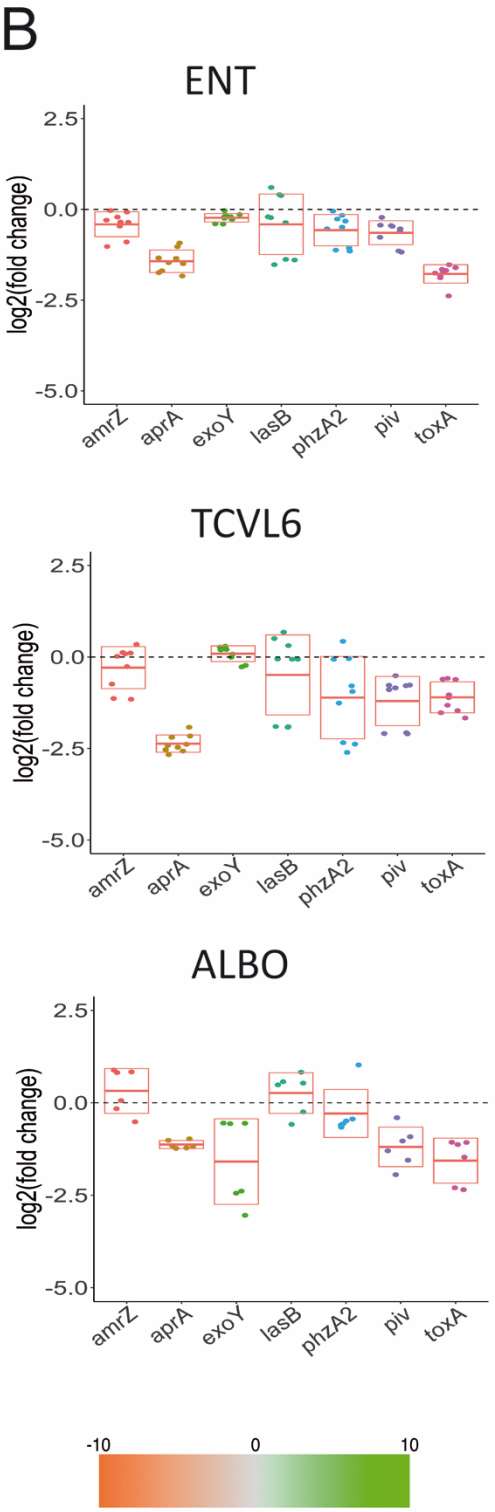

Fig 7. A. Analysis of changes in the expression of virulence factors in *P. aeruginosa* cells during A549 epithelial cell infection, in the presence or absence of FERRI, ALBO, ENT, TCV,

or TCVL6. Proteomic analyses were performed on *P. aeruginosa* PAO1 cells as in Fig 5. Median values measured in the infection assay supplemented with either 10 µM FERRI, ALBO, ENT, TCV, or TCVL6 were plotted against those measured in the infection assay in the absence of supplementation with siderophore or siderophore-antibiotic compounds. The median values represent the median of the relative intensity of each protein normalized against all proteins detected by shotgun analysis (n = 5).

B. Analysis of the changes in the transcription of genes encoding virulence factors in *P. aeruginosa cells* during A549 epithelial cell infection, in the presence or absence of ENT, TCVL6, or ALBO. RT-qPCR analyses were performed on the same infection assays as in Fig 4. The data were normalized relative to the reference gene *uvrD* and are representative of three independent experiments performed in triplicate (*n* = 3). Results are given as the ratio between the values obtained in the presence of siderophores or conjugates over those obtained in their absence. *amrZ* encodes a transcriptional regulator controlling many genes involved in environmental adaptation (41), *aprA,* an alkaline protease (40), *exoY* (56), *lasB,* an elastase (48), *phzA2,* a flavin-containing monooxygenase involved in phenazine biosynthesis (42, 43), *piv,* a lysyl-endopeptidase (also called PrpL) (38, 39) and *toxA,* an exotoxin (36, 37).

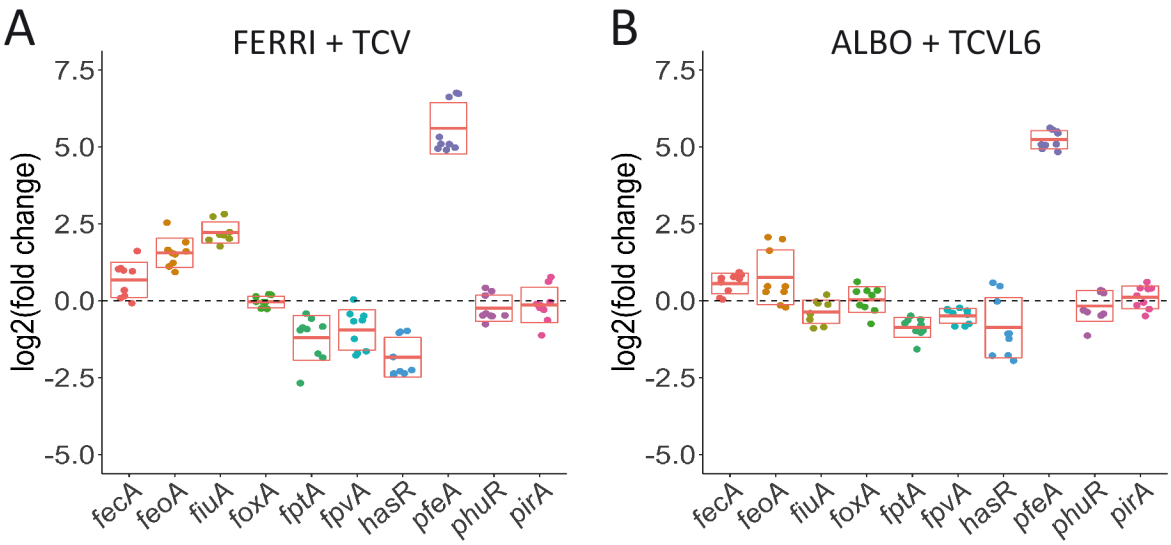

Fig 8. Analysis of the changes in the transcription of genes encoding OMTs involved in iron-uptake pathways in *P. aeruginosa cells* during A549 epithelial cell infection, in the presence or absence of a mixture of either FERRI and TCV or ALBO and TCVL6. RT-qPCR analyses were performed on *P. aeruginosa* PAO1 cells after 3 h of incubation with A549 epithelial cells in RPMI medium, with or without a mixture of two compounds: either FERRI and TCV or ALBO and TCVL6 (each of the compounds being present at a concentration of 10 µM). The data were normalized relative to the reference gene *uvrD* and are representative of three independent experiments, each performed in triplicate (n = 3). Results are given as the ratio between the values obtained in the presence of the conjugates over those obtained in their absence. *fecA* encodes the OMT of ferri-citrate, *feoA*, the ferrous transporter, and *fiuA*, the OMT of FERRI, *foxA,* that of ferrioxamine B, *fptA*, that of PCH, *fpvA*, that of PVD, *hasR* and *phuR*, that of heme, *pfeA* and *pirA*, that of ENT, and *piuA*, that of an unknown siderophore.

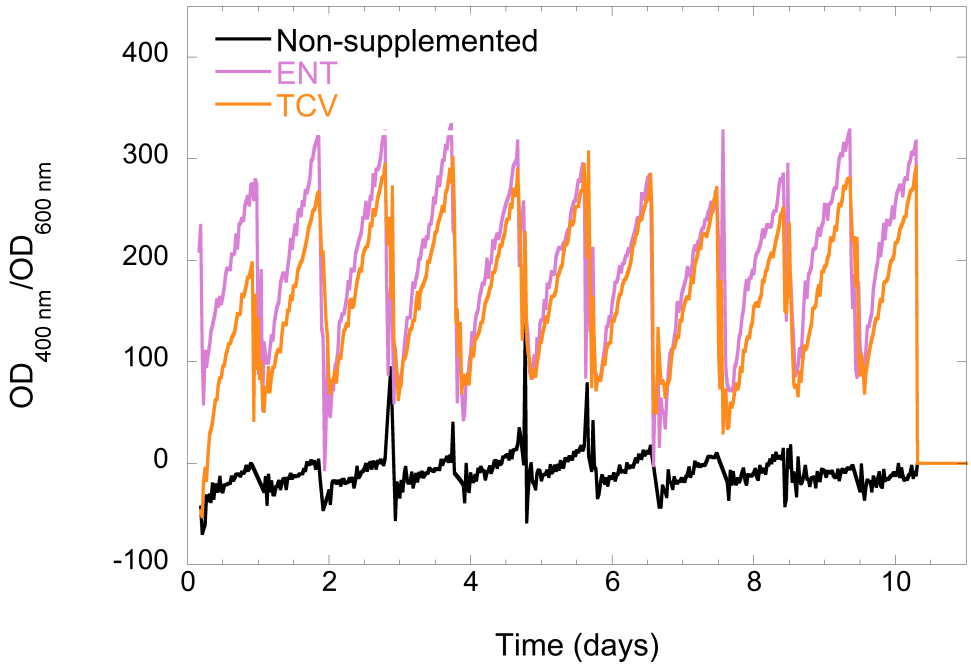

Fig 9. Monitoring the ENT-Fe uptake pathway via PfeEmCherry fluorescence during bacterial growth in the presence or absence of ENT or TCV. Fresh CAA medium was inoculated with *pfeEmcherry* (cells expressing fluorescent tagged PfeE) grown in the same medium and the resulting culture dispensed into the wells of a 96-well plate. ENT (kinetics in pink) or TCV (kinetics in orange) (10 µM) was added and a control experiment with no chelator was carried out in parallel (kinetics in black). $OD_{600\ nm}$ measurements were used to assess growth over time. The fluorescence of mCherry was measured at 610 nm (excitation at 570 nm). The measurements were performed at 30-min intervals in a TECAN microplate reader at 30°C, with shaking, for 11 days. Every 24 h, the plate was centrifuged, the supernatant removed, and new CAA media, with or without TCV or ENT, added and the plate returned to the microplate reader at 30°C with shaking. Each curve corresponds to the mean of three replicates.

Supporting information

S1 Table. Strains and plasmids used in this study.

Strain	Collection ID	Relevant characteristics	Reference
Pseudomonas aeruginosa			
PAO1	PAO1	Wild-type strain	
ΔpvdFΔpchA	PAS283	PAO1; *pvdF* and *pchA* chromosomally deleted	(1)
ΔpvdFΔpchAΔpfeA	PAS294	PAO1; *pvdF, pchA* and *pfeA* chromosomally deleted	(2)
ΔpvdFΔpchAΔpirA	PAS348	PAO1; *pvdF, pchA* and *pirA* chromosomally deleted	(1)
ΔpvdFΔpchAΔpfeAΔpirA	PAS351	PAO1; *pvdF, pchA, pfeA* and *pirA* chromosomally deleted	(1)
ΔpvdFΔpchAΔfiuA	PAS534	PAO1; *pvdF, pchA* and *fiuA* chromosomally deleted	(3)
pfeEmcherry	PAS355	PAO1; *pfeEmcherry* chromosomally integrated	(4)

S2 Table. Primers used for RT-qPCR analysis

Primer ID	Target	Sequence
uvrD F	*uvrD*	CTACGGTAGCGAGACCTACAACAA
uvrD R	*uvrD*	GCGGCTGACGGTATTGGA
GAPDH F	*GAPDH*	TGCACCACCAACTGCTTAGC
GAPDH R	*GAPDH*	GGCATGGACTGTGGTCATGAG
aprA F	*aprA*	AACCAGAAGATCAACCTCAACGA
aprA R	*aprA*	TCGACACATTGCCCTTCAAC
exoY F	*exoY*	AATGGATGGCGGAGCCTATA
exoY R	*exoY*	CAAGGCGTTGCCGAGAGAT
lasB F	*lasB*	CGCCTGGGCGAGAACA
lasB R	*lasB*	GGGAATCAGGTAGGAGACGTTGT
phzA2 F	*phzA2*	GGCACAACGTGCGGATCT
phzA2 R	*phzA2*	CGCACTCGACCCAGAAGTG

piv F	*piv*	GCGTGGGCCTGAAAACG
piv R	*piv*	CGATCCATTCGAGGGTTGTC
toxA F	*toxA*	CCCGGCGAAGCATGAC
toxA R	*toxA*	GGGAAATGCAGGCGATGA
amrZ F	*amrZ*	TCGCTCGCAGCCATCAC
amrZ R	*amrZ*	TCGAGTCGGGCGATGATC
fecA F	*fecA*	GATCGACGACCTGATCCTCAA
fecA R	*fecA*	GGTCATCGCCGAAAACGT
pirA F	*pirA*	GCCTGAACGCTTCCCAAA
pirA R	*pirA*	TGAAGGCCCGTGCGATA
pfeA F	*pfeA*	GCCGAGACCAGCGTGAAC
pfeA F	*pfeA*	GGCCGGATTCGATCTTGTT
fpvA F	*fpvA*	AGCCGCCTACCAGGATAAGC
fpvA R	*fpvA*	TGCCGTAATAGACGCTGGTTT
fptA F	*fptA*	GCGCCTGGGCTACAAGATC
fptA R	*fptA*	CCGTAGCGGTTGTTCCAGTT
foxA F	*foxA*	AAGGGCTCGGATACCCAGTT
foxA R	*foxA*	CGTTGGGATCGTGTTGCA
fiuA F	*fiuA*	GCCGCGACAAGAAGTTCAG
fiuA R	*fiuA*	ACGACTCCGCATAGGAGATATAGG
feoA F	*feoA*	CCTACCGCATCACCGGTTAT
feoA R	*feoA*	ACAGGCGTTGGCGATAGC
hasR F	*hasR*	AGCGCCTGCAGTTCAGCTA
hasR R	*hasR*	GTTCTCGGTGTTGAGCATGTTG
phuR F	*phuR*	GGTCGAACTGCCCAACGA
phuR R	*phuR*	TACGATGTCCGGATCGACGTA

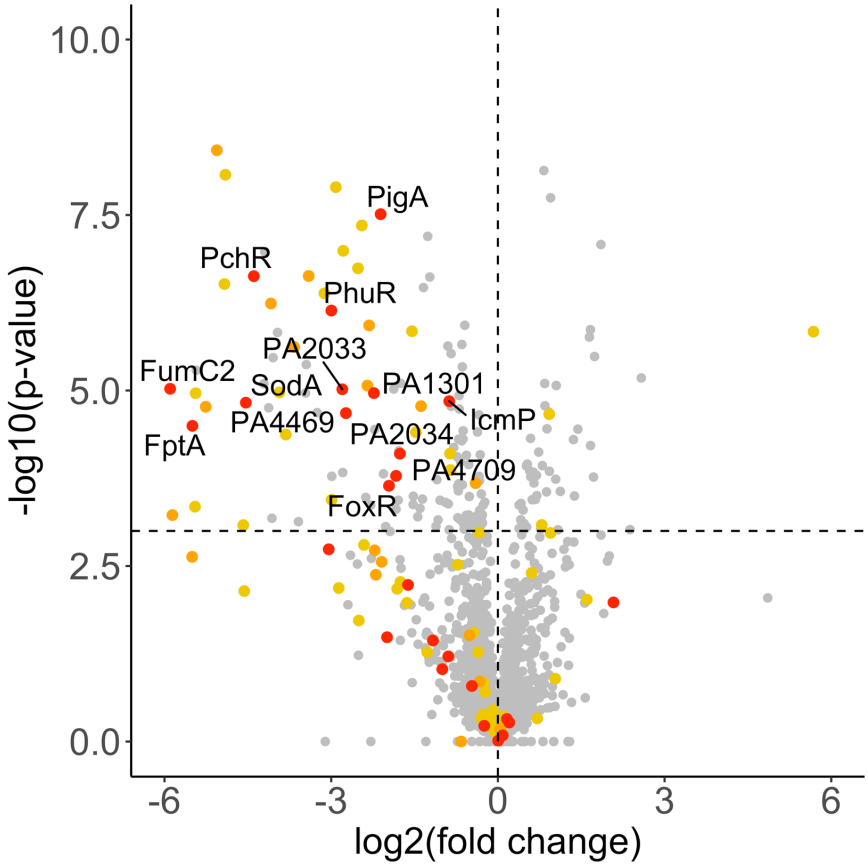

S1 Fig. Differential production of iron-regulated proteins in the presence of ALBO based on the Palma, Worgall, and Quadri (2003) and Ochsner et al. (2002) studies (5, 6). Both studies were transcriptome analyses of the *P. aeruginosa* response to iron. The analysis presented here was performed on *P. aeruginosa* PAO1 cells after a 3-h infection of A549 epithelial cells in RPMI medium, in the presence or absence of 10 µM ALBO. The yellow points correspond to proteins identified in one of the two analyses, the orange points to proteins identified in the two analyses, and the red points to proteins belonging to the direct Fur regulon, as described in the Collectf database.

Synthesis of TCVL6.

General informations

TCVL6 was synthesized as described in 1S Scheme. Linezolid was purchased from Sigma-Aldrich. Protected TCV **1** and linezolid-azide derivative **2** were synthesized according previously described protocols (7, 8). All reactions were carried out under argon (technical

quality, Air products). Solvents used were of analytical grade purity (>99.9%). When necessary, solvents and bases were purchased extra-dry. All other chemicals were obtained from commercial suppliers and were used as received, unless otherwise stated. All reactions were monitored by thin-layer chromatography (TLC) using *Merck* precoated silica gel $60F^{254}$ (0.25 mm). TLC are visualized using UV (254 nm/365 nm, *Vilber Lourmat*, VL-4LC) and/or using classical revelation mixtures (sulfuric vaniline, potassium permanganate, ninhydrin reagent). Final conjugate **3** was also detected on TLC using a 2% hydromethanolic solution of $FeCl_3$ (2%). Before chromatographic purification reaction mixtures were adsorbed on silica gel (60-200 µm, VWR Chemicals). Chromatographic purifications were performed on a *Reveleris* (*Grace Davison Discovery Sciences*) purification device using PuriFlash® pre-packed silica gel columns (Interchim, Montluçon, France). NMR spectra were recorded on Bruker Avance 400 (^{1}H: 400 MHz, ^{13}C: 100 MHz, ^{19}F : 376 MHz) or Avance 500 (^{1}H: 500 MHz, ^{13}C: 125 MHz, ^{19}F : 470 MHz), using the residual non-deuterated solvent as reference. The chemical shifts (δ) and coupling constants (J) are expressed in ppm and hertz respectively. Multiplicity is indicated as follow: s for singlet, d for doublet, t for triplet, q for quadruplet, quint for quintuplet and m for a multiplet. The letter "b" before the multiplicity indicate a broaden signal. Mass spectra were recorded in the *Service Commun d'Analyses* (SCA) *de la Faculté de Pharmacie de l'Université de Strasbourg* and were measured in ES-TOF experiments on a *Bruker Daltonic* MicroTOF mass spectrometer. LC/HRMS were measured after calibration on an *Agilent* QToF.

Protocol

Linezolid azide **2** (1 eq.) and alkyne-vector **1** (1,2 eq.) were solubilized in THF (final concentration 0.1 M). An aqueous solution of $CuSO_4$ (200 mg/mL, 1 eq.) and sodium ascorbate (5 eq.) were successively added (9). The mixture was sonicated and further stirred at 20°C

under argon till the total consumption of limiting reagent (linezolid azide). The mixture was then filtered through a celite pad and the filtrate was adsorbed on silical gel. The crude mixture was then purified on silica gel using a gradient of EtOH in CH_2Cl_2. The resulting white solid was dissolved in the mixture CH_2Cl_2/TFA/Triisopropylsilane/EtOH (70/20/5/5, 5 mL for 0.1 mmol of starting linezolid azide **2**). The solution was stirred at 20°C till the total consumption of the starting material. Solvents were then evaporated from the mixture under reduced pressure. The oily residue was dissolved in a minimum volume of THF then cyclohexane was added dropwise till the precipitation of the expected conjugate as a thin powder. The pure conjugate was filtered off on a Hirsch funnel.

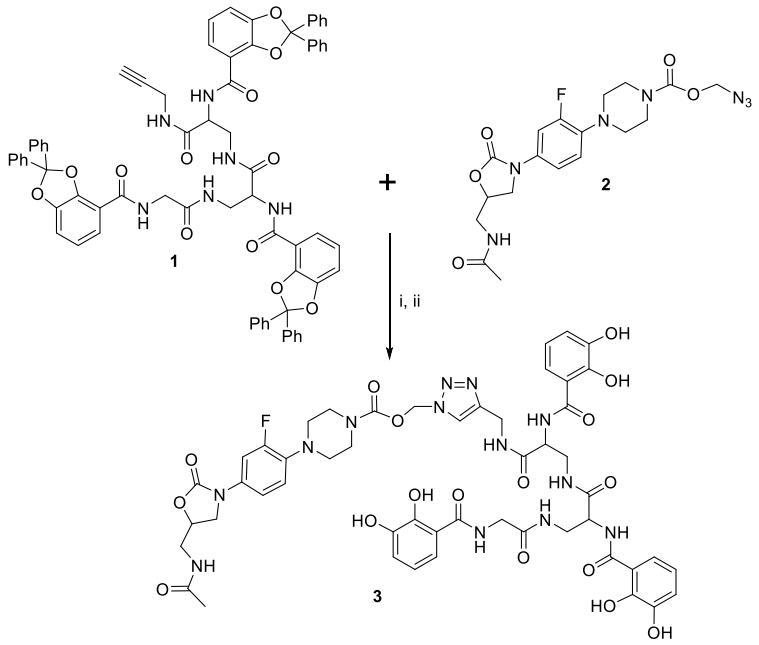

S1 Scheme: Synthesis of TCVL6 (3). i. $CuSO_4$, sodium ascorbate, THF/H_2O, (((, 20°C. ii. CH_2Cl_2/TFA/Triisopropylsilane/EtOH (70/20/5/5, 20°C.

Spectroscopic analysis of TCVL6.

^{1}H NMR (500 MHz, DMSO-d_6): δ 11.98 (s, 1H), 11.73 (m, 2H), 9.05 (br s, 3H), 8.79 (s, 1H), 8.56 (d, J = 6.9 Hz, 1H), 8.53 (d, J = 6.9 Hz, 1H), 8.45 (t, J = 5.5 Hz, 1H), 8.18 (t, J = 5.5 Hz, 1H), 8.02 (t, J = 5.5 Hz, 1H), 7.93 (t, J = 5.5 Hz, 1H), 7.81 (s, 1H), 7.46 (t, J = 7.2 Hz, 1H), 7.28-7.22 (m, 1H), 7.08-6.99 (m, 3H), 6.95-6.89 (m, 1H), 6.84-6.78 (m, 1H), 6.72-6.66 (m, 3H), 6.49-6.40 (m, 3H), 6.03 (s, 2H), 4.35-4.28 (m, 1H), 4.19-4.08 (m, 2H), 4.02-3.91 (m, 2H), 3.89-3.85 (m, 1H), 3.71-3.65 (m, 1H), 3.55-2.91 (m, 14H), 1.44 (s, 3H). **^{19}F NMR** (125 MHz, DMSO-d_6): δ -73.72, -121.19. **^{13}C NMR** (125 MHz, DMSO-d_6): δ 169.7, 169.6, 169.5, 169.4, 169.3, 169.2, 169.1, 162.5, 149.2, 149.0, 146.1, 146.0, 145.4, 137.1, 132.8, 129.7, 128.7, 124.1, 119.9, 118.9, 118.8, 118.2, 118.1, 117.8, 117.7, 115.5, 114.1, 71.6, 68.4, 53.9, 53.8, 53.7, 50.1, 47.3, 47.2, 43.7, 42.4, 41.5, 10.5, 40.3, 40.2, 40.1, 35.9, 30.9, 27.5, 23.4, 23.3, 22.5, 21.8, 21.7. **HRMS:** $C_{50}H_{54}FN_{13}O_{17}$: calcd: 1127.37447, found: 1127.37501.

LC-HRMS Spectra of compound 3 (TCVL6)

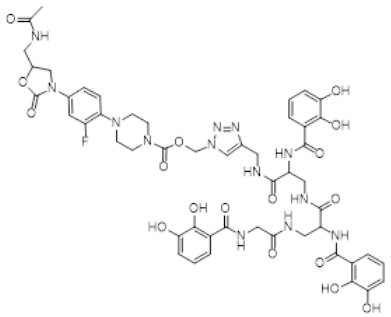

Data Filename	QT11799.d	**Sample Name**	NZ108
Inj. Vol.	0.1	**Position**	P1-B3
Instrument Name	SCA Illkirch QToF	**User Name**	PW
Acq Method	C18-2,1x5x1,8DMSO.m	**Acquired Time**	2/4/2016 12:07:19 PM
IRM Calibration Status	Success	**DA Method**	C18-2,1x5x1,8.m
Comment			

Sample Group **Info.**

User Chromatograms

Fragmentor Voltage 120 **Collision Energy** 0 **Ionization Mode** ESI

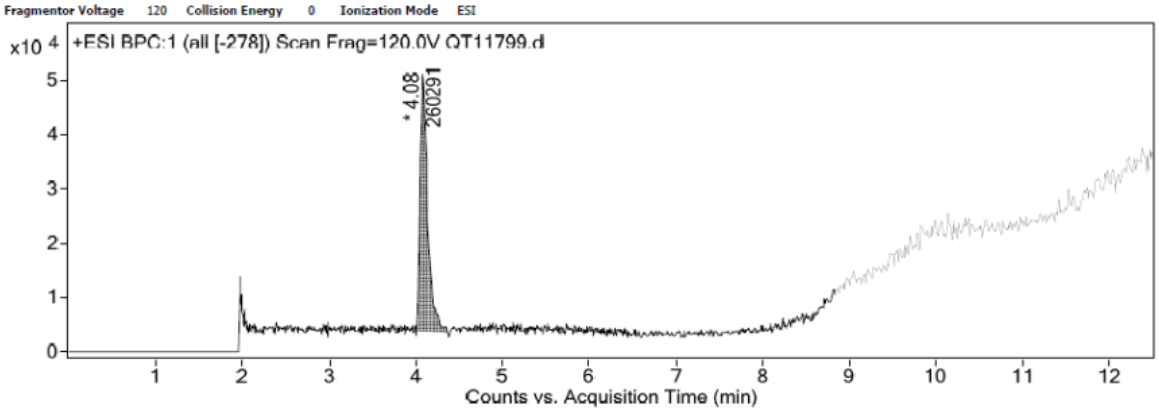

Integration Peak List

Start	RT	End	Height	Area	Area %	AreaSum%
3.97	4.08	4.37	47512	260291	100	100

946

947

948

Spectrum Source Peak (1) in "+ BPC:1 (all [-278]) Scan" **Fragmentor Voltage** 120 **Collision Energy** 0 **Ionization Mode** ESI

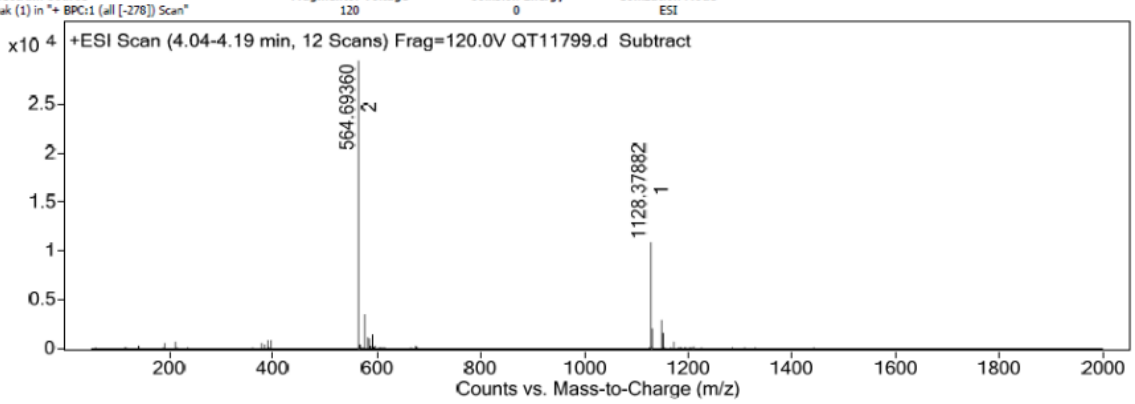

Peak List

m/z	z	Abund	Formula	Ion
564.6936	2	29418.6	C50 H56 F N13 O17	(M+2H)+2
565.19508	2	17423.8	C50 H56 F N13 O17	(M+2H)+2
565.69599	2	6106.5	C50 H56 F N13 O17	(M+2H)+2
575.68361	2	3582.9		
576.18663	2	2021		
1128.37882	1	10820.6	C50 H55 F N13 O17	(M+H)+
1129.38218	1	6280.4	C50 H55 F N13 O17	(M+H)+
1130.38535	1	2133	C50 H55 F N13 O17	(M+H)+
1150.36048	1	2936.7	C50 H54 F N13 Na O17	(M+Na)+
1151.36413	1	1682.2	C50 H54 F N13 Na O17	(M+Na)+

949

950

951

Formula Calculator Results

Formula	Best	Mass	Tgt Mass	Diff (ppm)	Mz	Ion Species	Score
C46 H50 F N19 O15		1127.37167	1127.37178	0.1	1128.37882	C46 H51 F N19 O15	99.57
C49 H49 N19 O14		1127.37166	1127.37064	-0.91	1128.37882	C49 H50 N19 O14	98.92
C45 H54 F N15 O19		1127.37165	1127.37044	-1.07	1128.37882	C45 H55 F N15 O19	98.77
C62 H50 F N11 O10		1127.3716	1127.37262	0.9	1128.37882	C62 H51 F N11 O10	98.03
C53 H53 N13 O16		1127.37162	1127.37332	1.51	1128.37882	C53 H54 N13 O16	97.9
C48 H53 N15 O18		1127.37164	1127.3693	-2.08	1128.37882	C48 H54 N15 O18	96.54
C50 H54 F N13 O17	TRUE	1127.37163	1127.37447	2.52	1128.37882	C50 H55 F N13 O17	95.18
C54 H49 N17 O12		1127.37164	1127.37466	2.68	1128.37882	C54 H50 N17 O12	94.19
C57 H50 F N13 O12		1127.37162	1127.36859	-2.68	1128.37882	C57 H51 F N13 O12	94.08
C51 H50 F N17 O13		1127.37165	1127.3758	3.69	1128.37882	C51 H51 F N17 O13	90.37
C46 H50 F N19 O15		1127.37139	1127.37178	0.34	1150.36048	C46 H50 F N19 Na O15	98.44
C49 H49 N19 O14		1127.37139	1127.37064	-0.66	1150.36048	C49 H49 N19 Na O14	98.12
C45 H54 F N15 O19		1127.37137	1127.37044	-0.82	1150.36048	C45 H54 F N15 Na O19	98.11
C48 H53 N15 O18		1127.37136	1127.3693	-1.83	1150.36048	C48 H53 N15 Na O18	96.2
C62 H50 F N11 O10		1127.37132	1127.37262	1.15	1150.36048	C62 H50 F N11 Na O10	96.17
C53 H53 N13 O16		1127.37134	1127.37332	1.76	1150.36048	C53 H53 N13 Na O16	96.08
C57 H50 F N13 O12		1127.37134	1127.36859	-2.43	1150.36048	C57 H50 F N13 Na O12	93.62
C50 H54 F N13 O17	TRUE	1127.37135	1127.37447	2.77	1150.36048	C50 H54 F N13 Na O17	93.18
C54 H49 N17 O12		1127.37136	1127.37466	2.92	1150.36048	C54 H49 N17 Na O12	92.17
C60 H49 N13 O11		1127.37133	1127.36745	-3.45	1150.36048	C60 H49 N13 Na O11	89.46
C53 H53 N13 O16		1127.37264	1127.37332	0.6	564.6936	C53 H55 N13 O16	99.64
C46 H50 F N19 O15		1127.3727	1127.37178	-0.81	564.6936	C46 H52 F N19 O15	99.61
C62 H50 F N11 O10		1127.37262	1127.37262	-0.01	564.6936	C62 H52 F N11 O10	98.85
C50 H54 F N13 O17	TRUE	1127.37265	1127.37447	1.61	564.6936	C50 H56 F N13 O17	98.67
C49 H49 N19 O14		1127.37269	1127.37064	-1.82	564.6936	C49 H51 N19 O14	98.32
C54 H49 N17 O12		1127.37267	1127.37466	1.77	564.6936	C54 H51 N17 O12	98.14
C45 H54 F N15 O19		1127.37267	1127.37044	-1.98	564.6936	C45 H56 F N15 O19	97.96
C51 H50 F N17 O13		1127.37267	1127.3758	2.78	564.6936	C51 H52 F N17 O13	96.21
C48 H53 N15 O18		1127.37267	1127.3693	-2.99	564.6936	C48 H55 N15 O18	95.76
C42 H53 N19 O19		1127.37271	1127.37651	3.37	564.6936	C42 H55 N19 O19	94.43

References

1. Gasser V, Baco E, Cunrath O, August PS, Perraud Q, Zill N, Schleberger C, Schmidt A, Paulen A, Bumann D, Mislin GLA, Schalk IJ. 2016. Catechol siderophores repress the pyochelin pathway and activate the enterobactin pathway in *Pseudomonas aeruginosa*: an opportunity for siderophore-antibiotic conjugates development. Environ Microbiol 18:819–832.
2. Paulen A, Gasser V, Hoegy F, Perraud Q, Pesset B, Schalk IJ, Mislin GLA. 2015. Synthesis and antibiotic activity of oxazolidinone-catechol conjugates against *Pseudomonas aeruginos*a. Org Biomol Chem 13:11567–11579.
3. Normant VP, Josts I, Kuhn L, Perraud Q, Fritsch S, Hammann P, Mislin GLA, Tidow H, Schalk IJ. 2020. Nocardamine-dependent iron uptake in *Pseudomonas aeruginosa:* exclusive

965 involvement of the FoxA outer membrane transporter. ACS Chem Biol.
966 4. Perraud Q, Moynié L, Gasser V, Munier M, Godet J, Hoegy F, Mély Y, Mislin GLA, Naismith
967 JH, Schalk IJ. 2018. A Key Role for the Periplasmic PfeE Esterase in Iron Acquisition via the
968 Siderophore Enterobactin in *Pseudomonas aeruginosa*. ACS Chem Biol 13:2603–2614.
969 5. Palma M, Worgall S, Quadri LEN. 2003. Transcriptome analysis of the *Pseudomonas*
970 *aeruginosa* response to iron. Arch Microbiol 180:374–379.
971 6. Ochsner UA, Wilderman PJ, Vasil AI, Vasil ML. 2002. GeneChip expression analysis of the
972 iron starvation response in *Pseudomonas aeruginosa*: identification of novel pyoverdine
973 biosynthesis genes. Mol Microbiol 45:1277–87.
974 7. Baco E, Hoegy F, Schalk IJ, Mislin GL. 2014. Diphenyl-benzo[1,3]dioxole-4-carboxylic acid
975 pentafluorophenyl ester: a convenient catechol precursor in the synthesis of siderophore
976 vectors suitable for antibiotic Trojan horse strategies. Organic & biomolecular chemistry
977 12:749–57.
978 8. Paulen A, Hoegy F, Roche B, Schalk IJ, Mislin GLA. 2017. Synthesis of conjugates between
979 oxazolidinone antibiotics and a pyochelin analogue. Bioorg Med Chem Lett 27:4867–4870.
980 9. Rostovtsev VV, Green LG, Fokin VV, Sharpless KB. 2002. A Stepwise Huisgen Cycloaddition
981 Process: Copper(I)-Catalyzed Regioselective “Ligation” of Azides and Terminal Alkynes.
982 Angewandte Chemie International Edition 41:2596–2599.
983
984
985